nature materials

SUPPLEMENTARY INFORMATION

DOI: 10.1038/NMAT4476

A small-molecule dye for NIR-II imaging

Alexander L. Antaris[1,2,†], Hao Chen[1,3,†], Kai Cheng[3], Yao Sun[1], Guosong Hong[2], Chunrong Qu[1], Shuo Diao[2], Zixin Deng[1], Xianming Hu[1], Bo Zhang[2], Xiaodong Zhang[2], Omar K. Yaghi[2], Zita R. Alamparambil[2], Xuechuan Hong[*1], Zhen Cheng[*3], Hongjie Dai[*2]

1. State Key Laboratory of Virology, Key Laboratory of Combinatorial Biosynthesis and Drug Discovery (Wuhan University), Ministry of Education, Wuhan University School of Pharmaceutical Sciences, Wuhan 430071, People's Republic of China
2. Department of Chemistry, Stanford University, California, 94305
3. Molecular Imaging Program at Stanford (MIPS), Bio-X Program, and Department of Radiology, Canary Center at Stanford for Cancer Early Detection, Stanford University, California, 94305-5344

† These authors contributed equally

*Correspondence should be sent to: hdai@stanford.edu, zcheng@stanford.edu or xhy78@whu.edu.cn

A. General Synthesis Information.

All air and moisture sensitive reactions were carried out in flame-dried glassware under a nitrogen atmosphere. Reactive liquid compounds were measured and transferred by gas-tight syringes and were added in the reaction flask through rubber septa. Tetrahydrofuran (THF) were freshly distilled from sodium benzophenoneketyl. Dichloromethane, tolueneand DMF were distilled from CaH_2. Sulfo-SMCC (Sulfosuccinimidyl 4-[*N*-maleimidomethyl]cyclohexane-1-carboxylate) was purchased from Thermo Scientific (Rockford, IL). PEG_{2000}-NH_2. All other standard synthesis reagents were purchased from Sigma-Aldrich Chemical Co. (St. Louis, MO) and used without further purification. The cell line was obtained from the American Type Tissue Culture Collection (Manassas, VA). Female athymic nude mice (nu/nu) were purchased from Charles River Laboratories (Boston, MA).4,4'-(Phenylazanediyl) dibenzaldehyde(**1**)[1], 4,7-dibromo-5,6-dinitrobenzo[c][1,2,5]thiadiazole(**7**)[2], Affibody Ac-Cys-$Z_{EGFR:1907}$: (Ac-CVDNKFNKEMWAAWEEIRNLPNLNGWQMTAFIASLVDDPSQSANLLAEAKKLNDAQAPK-NH_2)[3] were prepared according to literature methods.

Analytical thin layer chromatography was performed on glass-backed silica gel plates with F_{254} indicator. Compounds were visualized under UV lamp or by developing in iodine, vanillin, phosphomolybdic acid solution or with a potassium permanganate solution followed by heating on a hot plate to approximately 350 °C. Flash chromatography was performed on 230-400 mesh silica gel with technical grade solvents which were distilled prior to use. ^{1}H NMR spectra were recorded on a Bruker AV400 at 400 MHz as $CDCl_3$ solutions with tetramethylsilane (δ = 0 ppm) as the internal standard. ^{13}C spectra were obtained on the same instruments at 100 MHz with $CDCl_3$ (δ = 77 ppm) as the internal reference. Chemical shifts are reported in parts per million (ppm). Multiplicities are reported as s (singlet), d (doublet), t (triplet), q (quartet), m (multiplet), dd (doublet of doublet), etc. High-resolution mass spectra were performed on Bruker APEX III 7.0 Tesla Ion Spec 4.7 Tesla FTMS and Thermo Scientific LTQ ORBITRAP XL. Matrix assisted laser desorption/ionization time of flight mass spectrometry (MALDI-TOF-MS) by Stanford Protein and Nucleic Acid Biotechnology Facility, Stanford University. Analytical or preparative high performance liquid chromatography (HPLC) was performed on a DIONEX ultimate 3000 instrument with PDA detection (column: PrincetonSPHER-300 C_{18}, 5μ, 250 mm × 4.6 mm or 10.0 mm; mobile phase: water/acetonitrile with 0.1 % TFA).

B. Experiment

Figure S1: Synthesis of CH1055.

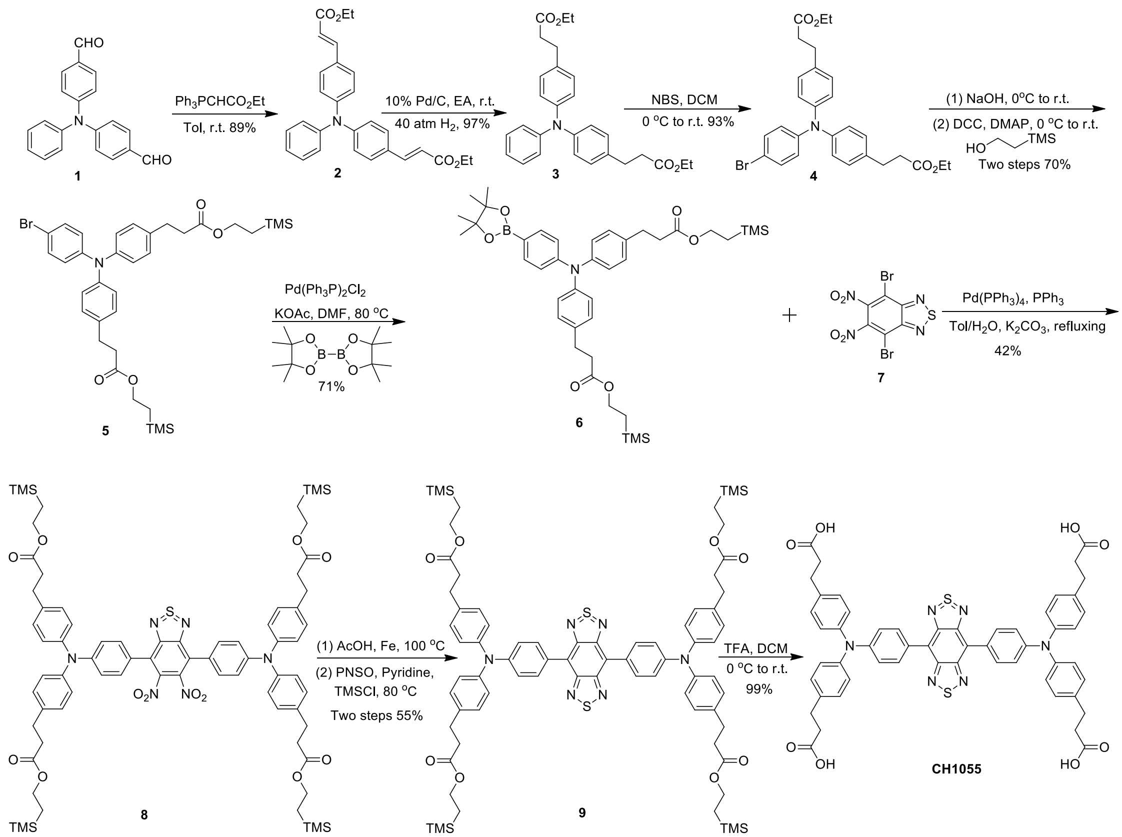

(1) Synthesis of (2E,2'E)-diethyl 3,3'-((phenylazanediyl)bis(4,1-phenylene))diacrylate (**2**)

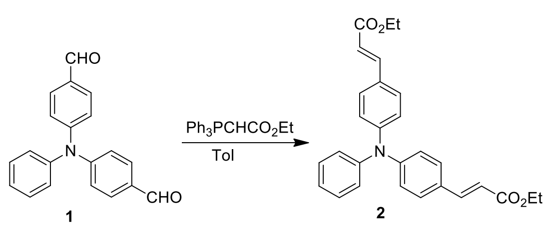

Ethyl (triphenylphosphoranylidene) acetate (26.13 g, 75 mmol) was added to a solution of aldehyde **1** (10.27 g, 34.1 mmol) in anhydrous toluene (100 mL) under an inert atmosphere (N_2). The solution was stirred for 48 hours at room temperature. The reaction mixture was concentrated *in vacuo* and the residue was purified by silica gel chromatography (petroleum ether: EtOAc = 16:1 v/v) to give a bright yellow oil **2** (13.4 g, 89% yield). ^{1}H NMR (400 MHz, $CDCl_3$) δ 7.64 (d, J = 16.0 Hz, 2H), 7.41 (d, J = 8.6 Hz, 4H), 7.32 (t, J = 7.8 Hz, 2H), 7.15 (t, J = 7.7 Hz, 3H), 7.07 (d, J = 8.5 Hz, 4H), 6.34 (d, J = 15.9 Hz, 1H), 4.27 (q, J = 7.1 Hz, 4H), 1.34 (t, J = 7.1 Hz, 6H).^{13}C NMR (101 MHz, $CDCl_3$) δ 167.2, 148.9, 146.4, 143.9, 129.73, 129.3, 128.9, 126.0, 124.8, 123.3, 116.4, 60.4, 14.4.HRMS (ESI) Calcd for: $C_{28}H_{28}NO_4^+$([M+H]$^+$): 442.2013. Found: 442.2000.

(2) Synthesis of diethyl 3,3'-((phenylazanediyl)bis(4,1-phenylene))dipropanoate(**3**)

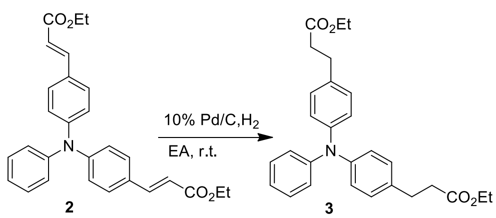

A mixture of **2** (6.462 g, 14.6 mmol) and 10% Pd/C (0.64 g) in EtOAc (100 mL) was evacuated and back-filled with H_2 (40 atm).After stirring 24 hours at room temperature, the mixture was filtered over a pad of Celite (EtOAc eluent) and the solvent was evaporated *in vacuo*. The crude product was further purified by silica gel chromatography (petroleum ether : EtOAc = 16:1 v/v) to afford a colorless oil **3** (6.28 g, 97% yield).^{1}H NMR (400 MHz, $CDCl_3$) δ 7.09 (t, J = 7.8 Hz, 2H), 7.00 – 6.80 (m, 11H), 4.03 (q, J = 7.1 Hz, 4H), 2.80 (t, J = 7.8 Hz, 4H), 2.50 (t, J = 7.8 Hz, 4H), 1.14 (t, J = 7.1 Hz, 6H).^{13}C NMR (101 MHz, $CDCl_3$) δ 173.0, 148.0, 146.1, 134.9, 129.1, 129.1, 124.3, 123.6, 122.3, 60.4, 36.0, 30.4, 14.3. HRMS (ESI) Calcd for: $C_{28}H_{32}NO_4^+$ ([M+H]$^+$): 446.2326. Found: 446.2325.

(3) Synthesis of diethyl 3,3'-(((4-bromophenyl)azanediyl)bis(4,1-phenylene))dipropanoate(**4**)

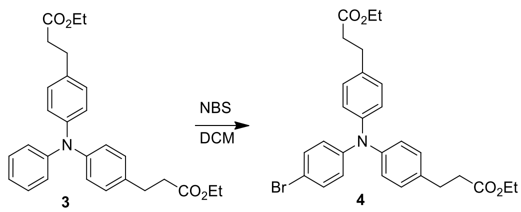

To 150 mL of DCM in 500 mL round bottomed flask was added compound **3** (5.28 g, 11.9 mmol). After stirring at 0~5 ^{o}C for 5 min, NBS (2.25 g, 12.61 mmol) was added in 5 portions. The reaction mixture was warmed to room temperature and stirred for additional 16 hours. The reaction was then completed and filtered through a pad of Celite and concentrated *in vacuo*, to give a brown oil. Purification of the crude product by flash chromatography (petroleum ether : EtOAc = 16:1 v/v) afforded a colorless oil **4** (5.8 g, 93% yield). ^{1}H NMR (400 MHz, $CDCl_3$) δ 7.25 (d, J = 8.7 Hz, 2H), 7.06 (d, J = 8.3 Hz, 4H), 6.96 (d, J = 8.4 Hz, 4H), 6.87 (d, J = 8.8 Hz, 2H), 4.13 (q, J = 7.1 Hz, 4H), 2.89 (t, J = 7.7 Hz, 4H), 2.60 (t, J = 7.8 Hz, 4H), 1.23 (t, J = 7.1 Hz, 6H).^{13}C NMR (101 MHz, $CDCl_3$) δ 173.0, 147.1, 145.5, 135.5, 132.0, 129.2, 124.5, 124.5, 114.3, 60.4, 35.9, 30.4, 14.2. HRMS (ESI) Calcd for: $C_{28}H_{31}BrNO_4^+$($[M+H]^+$): 524.1431. Found: 524.1404.

(4) Synthesis of bis(2-(trimethylsilyl)ethyl)3,3'-(((4-bromophenyl)azanediyl)bis(4,1-phenylene)) dipropanoate (**5**)

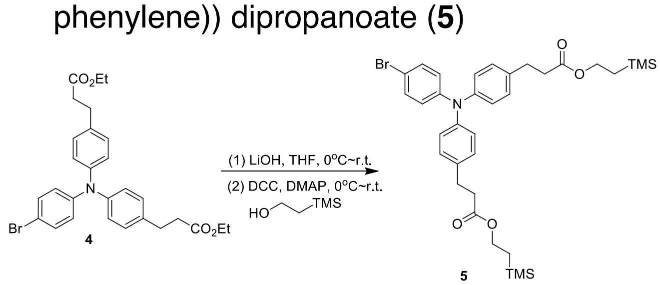

To 250 mL round bottomed flask was charged with compound **4** (4.271 g, 8.143 mmol), THF (120 mL), and the resulting solution was chilled to 0-5 ^{o}C in an ice bath. A solution of LiOH (0.9772 g, 40.715 mmol) in H_2O (40 mL) was added and the reaction mixture was stirred at 0-5 ^{o}C for 1 hour and then warmed to ambient temperature. The reaction was monitored by TLC analysis and it was completed in 24 hours monitor. The reaction mixture was acidified to pH 3 with sat. aq. $KHSO_4$ solution, extracted with EtOAc (3 ×100 mL). The combined organic extracts were dried over anhydrous $MgSO_4$ and concentrated *in vacuo*. The crude product was used for the next step without further purification.

To a solution of the acid in CH_2Cl_2 (80 mL) was added 4-dimethylaminopyridine (199 mg, 1.63 mmol), *N,N'*-dicyclohexylcarbodiimide (4.2 g, 20.36 mmol) and 2-(trimethylsilyl)ethanol (2.41 g, 20.36 mmol). The reaction was stirred at room temperature for 24 hours. The crude material was filtered through a medium porosity frit and volatiles were removed under reduced pressure. Purification of the crude product by silica gel chromatography (petroleum ether : EtOAc = 32:1 v/v) afforded a colorless oil **5** (3.81 g, 70% yield). ^1H NMR (400 MHz, $CDCl_3$) δ 7.26 (d, J = 8.8 Hz, 2H), 7.08 (d, J = 8.4 Hz, 4H), 6.97 (d, J = 8.4 Hz, 4H), 6.89 (d, J = 8.8 Hz, 2H), 4.24 – 4.16 (m, 4H), 2.91 (t, J = 7.7 Hz, 4H), 2.60 (t, J = 7.8 Hz, 4H), 1.04 – 0.97 (m, 4H), 0.06 (s, 18H). ^{13}C NMR (101 MHz, $CDCl_3$) δ 172.9, 147.1, 145.5, 135.6, 132.0, 129.3, 124.5, 114.2, 62.6, 36.0, 30.4, 17.3, -1.4. HRMS (ESI) Calcd for: $C_{34}H_{47}BrNO_4Si_2^+$ ($[M+H]^+$): 668.2222. Found: 668.2232

(5) Synthesis of compound **6**

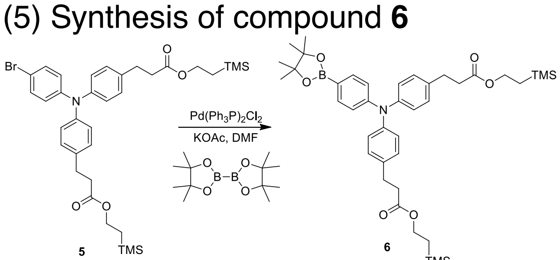

To a solution of bis(triphenylphosphine)palladium(II) dichloride(129 mg, 0.175 mmol), KOAc (413 mg, 4.21 mmol), and bis(pinacolate)diboron (535 mg, 2.11 mmol) in DMF (20 mL) was added compound **5** (1.173 g, 1.754 mmol) under an inert atmosphere (Ar). The reaction mixture was heated in an oil bath at 80 ^oC for 12 hours. The solution was cooled, dilute with H_2O (40 mL) and extracted with EtOAc (3 ×50 mL). The combined organic layers were washed with water (2 ×20 mL), dried over anhydrous $MgSO_4$ and evaporated *in vacuo*. The residue was purified by column chromatography (petroleum ether : EtOAc = 8:1 v/v) to give compound **6** (892 mg, 71% yield) as a colorless oil. ^{1}H NMR (400 MHz, $CDCl_3$) δ 7.66 (d, J = 8.5 Hz, 2H), 7.11 (d, J = 8.5 Hz, 4H), 7.05 – 6.99 (m, 6H), 4.23 – 4.17 (m, 4H), 2.93 (t, J = 7.8 Hz, 4H), 2.62 (t, J = 7.8 Hz, 4H), 1.35 (s, 12H), 1.03 – 0.98 (m, 4H), 0.07 (s, 18H).^{13}C NMR (101 MHz, $CDCl_3$) δ 173.1, 150.7, 145.5, 135.8, 135.7, 129.2, 125.1,121.2, 83.5, 62.7, 36.1, 30.4, 24.9, 17.3, -1.4. HRMS (ESI) Calcd for: $C_{40}H_{59}BNO_6Si_2^+$($[M+H]^+$): 716.3968.Found: 716.3941.

(6) Synthesis of compound **8**

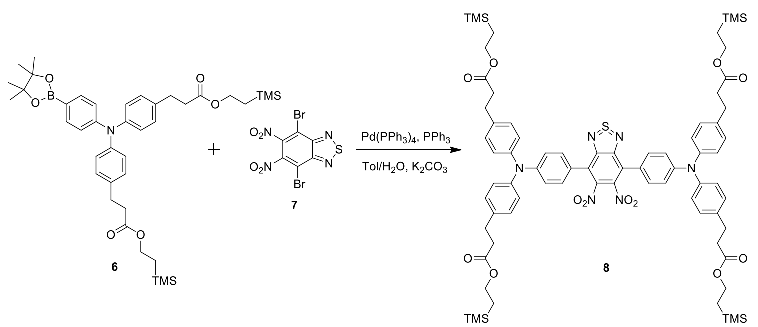

A 50 mL three-necked flask was charged with compound **6** (1.124 g, 1.57 mmol), compound **7** (250 mg, 0.654 mmol), and $Pd(PPh_3)_4$ (75 mg, 0.065 mmol), aqueous K_2CO_3 (1 M, 5 mL)in toluene (20 mL) under an inert atmosphere (Ar). The resulting mixture was further degassed with an Ar stream for 20 min and heated in an oil bath at 115-120 ^{o}C for 48 hours. The reaction was allowed to cool to room temperature and extracted with EtOAc (2 ×20 mL). The combined organic layers were washed with water (50 mL) and sat. brine (100 mL). After drying over anhydrous Mg_2SO_4 and removal of the solvents under reduced pressure, the residue was purified by column chromatography on silica gel (petroleum ether : EtOAc = 8:1 v/v) to yield the product as a red semi-solid (385 mg, 42% yield).^{1}H NMR (400 MHz, $CDCl_3$) δ 7.47 – 7.38 (m, 4H), 7.20 – 7.07 (m, 20H), 4.24 – 4.18 (m, 8H), 2.96 (t, J = 7.8 Hz, 8H), 2.64 (t, J = 7.8 Hz, 8H), 1.04 – 0.98 (m, 8H), 0.06 (d, J = 2.4 Hz, 36H).^{13}C NMR (101 MHz, $CDCl_3$) δ 173.1, 153.2, 149.9, 144.7, 142.2, 136.9, 130.2, 129.5, 127.8, 126.1, 121.8, 120.0, 62.7, 36.0, 30.4, 17.3, -1.4. HRMS (ESI) Calcd for: $C_{74}H_{93}N_6O_{12}SSi_4^+$([M+H]$^+$): 1401.5644. Found: 1401.5621.

(7) Synthesis of compound **9**

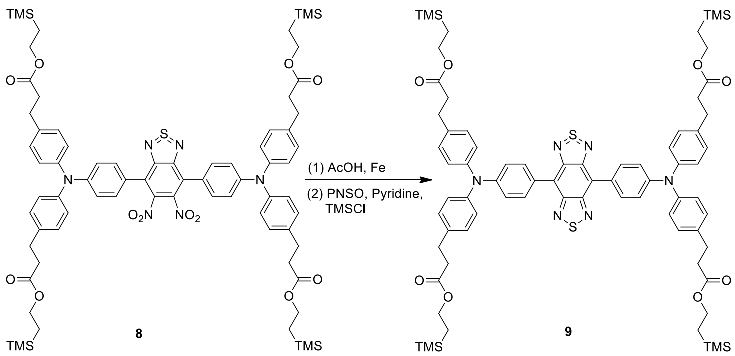

To a 10 mL sealed tube was added compound **8** (60 mg, 0.0428 mmol), iron powder (24 mg, 0.428 mmol), AcOH (4 mL). The reaction mixture was heated to 100 °C for 6 hours and then cooled to room temperature. The reaction solution was changed from red to yellow. The reaction was neutralized with sat. $NaHCO_3$ and extracted with EtOAc (2 ×10 mL). The combined organic layers were washed with water (10 mL), dried over anhydrous $MgSO_4$ and evaporated *in vacuo*. The resulting brown oil was used for the next step without further purification.

To a brownish solution in anhydrous pyridine (4 mL) was added *N*-thionylaniline (12.5 mg, 0.09 mmol) and TMSCl (46.5 mg,0.428 mol).The solution was heated in an oil bath at 80 ^{o}C for 16 hours. The reaction was allowed to cool, poured into iced water, extracted with EtOAc (2 ×10 mL). The combined organic layers were washed with water (10 mL), dried over anhydrous $MgSO_4$ and evaporated *in vacuo*. The residue was purified by column chromatography on silica gel (petroleum ether : EtOAc = 16:1 v/v) to yield the product **9** as a green semi-solid (32 mg, 55% yield).^{1}H NMR (400 MHz, $CDCl_3$) δ 8.19 (d, *J* = 8.8 Hz, 4H), 7.25 (d, *J* = 8.8 Hz, 4H), 7.22 – 7.13 (m, 16H), 4.26 – 4.18 (m, 8H), 2.96 (t, *J* = 7.8 Hz, 8H), 2.65 (t, *J* = 7.8 Hz, 8H), 1.05 – 0.99 (m, 8H), 0.07 (s, 36H).^{13}C NMR (101 MHz,$CDCl_3$) δ 173.0, 152.7, 148.4, 145.3, 136.1, 132.6, 129.3, 128.0, 125.6, 121.0, 120.1, 62.7, 36.1, 30.4, 17.3, -1.5. HRMS (ESI) Calcd for: $C_{74}H_{93}N_6O_8S_2Si_4^+$([M+H]$^+$): 1369.5568. Found: 1369.5284.

(8) Synthesis of compound **CH1055**

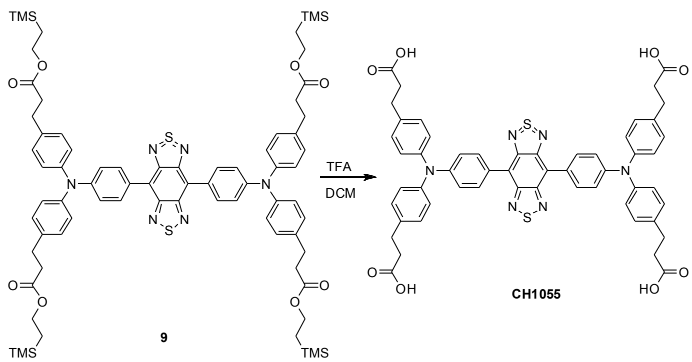

To a solution of compound **9** (10 mg, 0.0073 mg) in DCM (1 mL) was added TFA (1 mL) 0^{o}C. The reaction mixture was slowly warmed to ambient temperature. The reaction was completed in 30 min by TLC analysis. The solvent was removed *in vacuo* and the crude product was washed by acetonitrile (5 ×5 mL)to yield the desired product **CH1055** as a green semi-solid (7 mg, 99%). ^{1}H NMR (400 MHz, DMSO) δ 8.10 (d, *J* = 7.9 Hz, 4H), 7.24 (d, *J* = 7.6 Hz, 8H), 7.08 (d, *J* = 7.8 Hz, 12H), 2.83 (t, *J* = 7.1 Hz, 8H), 2.56 (t, *J* = 7.4 Hz, 8H).^{13}C NMR (101 MHz, DMSO) δ 174.2, 152.4, 148.2, 145.1, 136.9, 133.4, 130.0, 128.4, 125.4, 120.8, 119.5, 35.6, 30.2.HRMS (ESI) Calcd for: $C_{54}H_{45}N_6O_8S_2^+$ ([M+H]$^+$): 969.2735.Found: 969.2734

Synthesis of CH1055-PEG

To a solution of CH1055 (1 mg, 1.032 μmol) in 250 μL DMSO was added NH_2-PEG (20.64mg, 10.32 μmol, M.W. 2000, Laysan Bio), DIPEA 50μL, EDC (1.6mg, 10.32μmol) and NHS(1.19 mg, 10.32 μmol) . The reaction mixture was stirred 6h at room temperature then purified by Amicon Ultra-0.5mL 3k (washed 6 times). The purity of CH1055-PEG was controlled by HPLC (Thermo Scientific Hypersil GOLD C4 column). The final product CH1055-PEG was confirmed using MALDI-TOF-MS. Expected M.W. 9000 , Measured M.W. 9058

Figure S2: MALDI of CH1055-PEG

CH1055-PEG

Expected M.W. about 9000

Measured M.W. about 9058

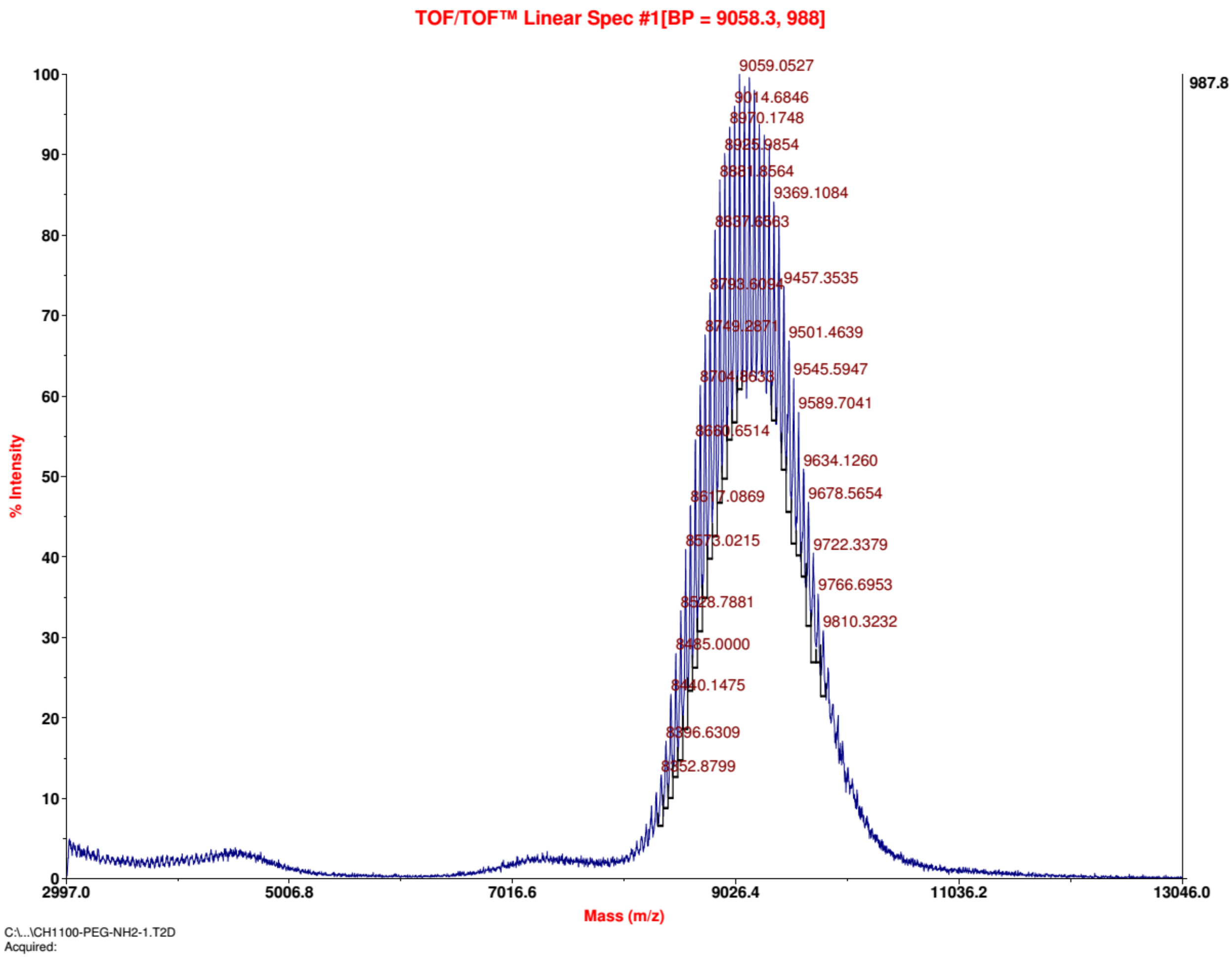

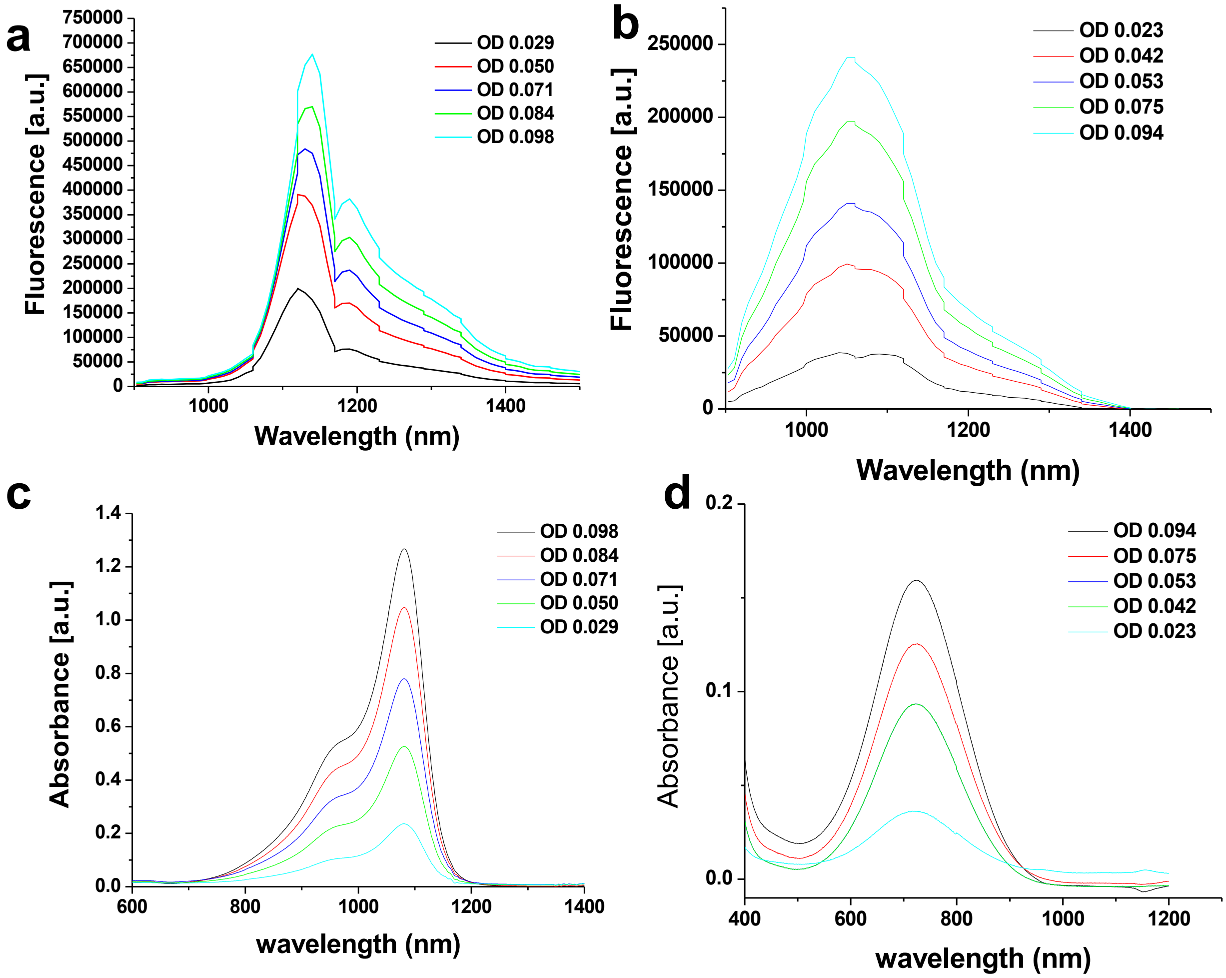

Figure S3: Quantum yield of CH1055-PEG. Fluorescence of (**a**) IR-26 and (**b**) CH1055-PEG and absorbance of (**c**) IR-26 and (**d**) CH1055-PEG. All fluorescence was collected on an InGaAs Princeton Instruments 1D array with an 808 nm laser for an excitation source and 900 nm LP filter. Absorbance was collected on a Cary 5000. The optical density values associated each spectra corresponds to the absorbance at 808 nm.

In order to measure the quantum yield of CH1055-PEG, a reference fluorophore emitting in the NIR-II was chosen. While there is some debate over the true quantum yield of IR-26, 0.5% is the accepted value. The quantum yield was calculated in the following manner:

$$QY = QY_{ref} \times \frac{n^2}{n_{ref}^2}\left(\frac{A_{ref}}{I_{ref}}\right)\frac{I_{sample}}{A_{sample}}$$

Instead of comparing the integrated fluorescence intensity at a single concentration to that of the reference, 5 difference concentrations at or below OD 0.1 (roughly OD 0.1, 0.08, 0.06, 0.04, and 0.02) were measured and the integrated fluorescence was plotted against absorbance for both IR-26 and CH1055-PEG. Comparison of the slopes led to the determination of the quantum yield of CH1055-PEG.

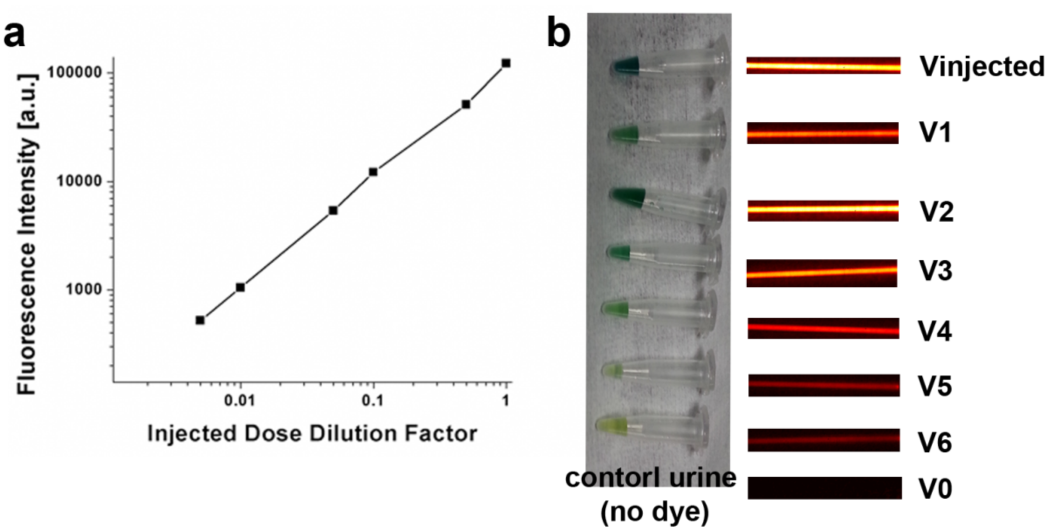

Figure S4: Measuring CH1055-PEG excretion in urine. (**a**)The linearity of the fluorescence emission was verified by checking average fluorescence intensity of the injected biodistribution dose and then a series of dilutions. (**b**) Urine was collected in capillarity tubes and the average fluorescence measured with an InGaAs 2D camera at an exposure time of 30 ms.

Before solely using the fluorescence of the excreted CH1055-PEG to measure the amount of excreted dye per mouse, the fluorescence intensity of the injected dose and a series of dilutions in PBS were measured in order to check the linearity. At higher concentrations, non-linear relationships between fluorescence and concentration occur due to variety of reasons such as inter-sample quenching effects. Within the above concentration range, the relationship between fluorescence intensity and concentration was linear as demonstrated below:

- To determine linearity and starting with a generalized formula:

$$y = a * x^k$$

becomes the following on a log-log plot:

$$\log(y) = \log(a) + k * \log(x)$$

- The slope on a log-log plot will determine whether the function is linear or follows an exponential relationship. Selecting two points:

$$\log[F(x_1)] = m * \log(x_1) + b$$
$$\log[F(x_2)] = m * \log(x_2) + b$$
$$m = \frac{\log(F_2) - \log(F_1)}{\log(x_2) - \log(x_1)}$$
$$m = \frac{\log\left(\frac{F_2}{F_1}\right)}{\log\left(\frac{x_2}{x_1}\right)}$$

where m = k is the slope of the line on the log-log plot which corresponds to the power of the generalized equation $y = a * x^k$.

- As m = 1.0 from the linearity check, y = a*x and there is a linear dependence between concentration and fluorescence intensity within this concentration range.

The %ID was measured in the following way:

$$\%ID = \frac{\sum_{m=1}^{m=s_f}\left((I_m - I_{control}) * V_m\right)}{\left(I_{injected} - I_{control}\right) * V_{injected}}$$

where s is the number of a urine time-point from a particular mouse starting at the first urine time-point collected s_1 until s_f, the last urine time-point collected, I is the average fluorescent intensity as measured with a 1200LP filter, $I_{control}$ is the fluorescent intensity of control urine at the same exposure time as the sample I_n, $I_{injected}$ is the fluorescent intensity of the injected dose, and V is the volume of the urine, and $V_{injected}$ is the volume of the injected CH1055-PEG.

The agglomerate cumulative excretion profile was formulated in the following way:

- The urine excretion time (t), volume (V), and fluorescence intensity (I) were gathered from all mice in the excretion study (n = 5).
- The excretion time (t), volume (V), and fluorescence intensity (I) from all the mice used in the study was rearranged in the following way:

$$\begin{pmatrix} t_1 & I_1 & V_1 \\ \vdots & \ddots & \vdots \\ t_f & I_f & V_f \end{pmatrix}$$

with the sample number $s_1$at $t_1$corresponding to the earliest urine time-point out of all the mice in the study ands_f att_f corresponding the last time-point out of all the mice in the study.

- The $\%ID_{total\ (n=5)}$ was calculated in the following way:

$$\%ID_{total\ (n=5)} = \frac{\sum_{m=1}^{m=s_f}\left((I_m - I_{control}) * V_m\right)}{\sum_{n=1}^{n=5}\left(\left((I_{injected} - I_{control}) * V_{injected}\right)_n\right)}$$

where s is the number of a urine time-point from all the mice in the study starting at the first urine time-point collected s_1 until s_f, the last urine time-point collected, I is the average fluorescent intensity as measured with a 1200LP filter, $I_{control}$ is the fluorescent intensity of control urine at the same exposure time as the sample I_n, $I_{injected}$ is the fluorescent intensity of the injected dose, and V is the volume of the urine, and $V_{injected}$ is the volume of the injected CH1055-PEG, and n corresponds the number of a mouse used in the study.

- The agglomerate excretion curve treats all of the individual mice as one system (or a 'super-mouse') and measures the total CH1055-PEG injected and all of the urine excreted from all of the mice.
- This was deemed the easiest way to portray the urine excretion data since urine was collected without coercion and time-points vary between mice.

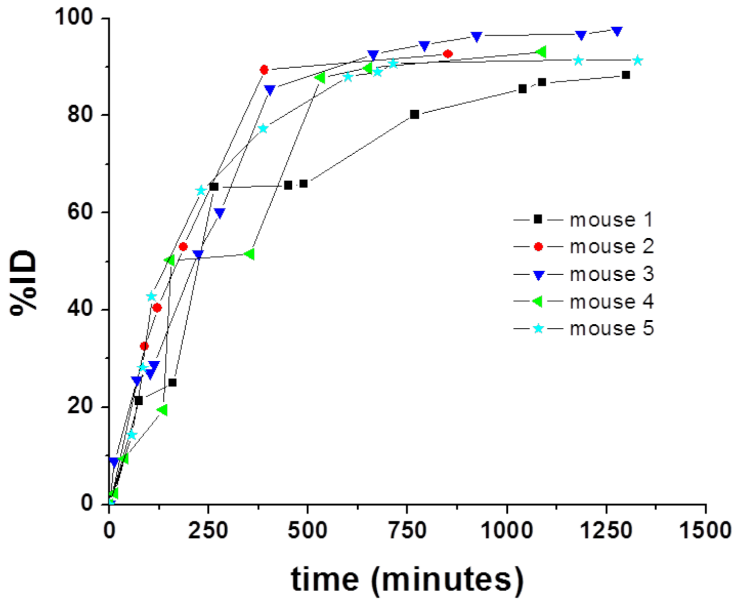

Figure S5: CH1055-PEG urine excretion from individual balb/c mice. Excretion profiles from the 5 individual mice used in the excretion study over the course of 24 hours.

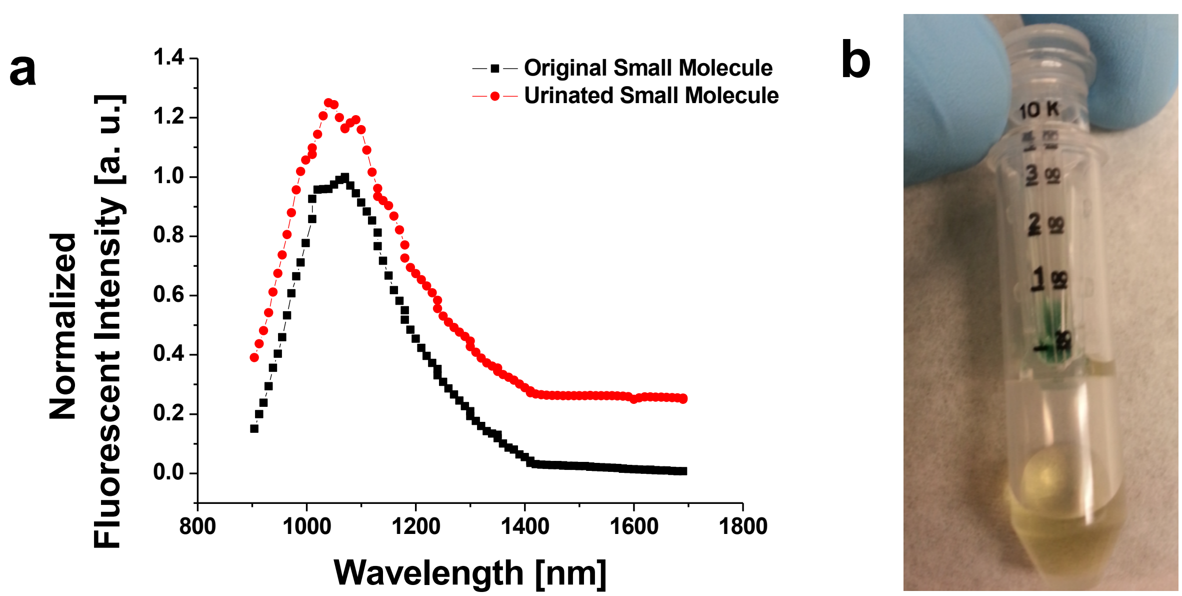

Figure S6: Characterization of CH1055-PEG excreted in urine. After collecting the urine excreted from a mouse, the CH1055-PEG was washed extensively to remove any small inorganic and organic compounds such as urea and dissolved ions with a 10K centrifuge filter. A fluorescence spectrum of the excreted CH1055-PEG was obtained by exciting the sample with a 808 nm excitation laser and collecting the emission with an InGaAs 1D spectrometer. No noticeable shift in the emission peak was noted, indicating that metabolism or degradation of the rapidly excreted CH1055-PEG is unlikely. However, residual low levels of CH1055-PEG that remain for longer periods of time *in vivo* may be metabolized and further investigation is necessary.

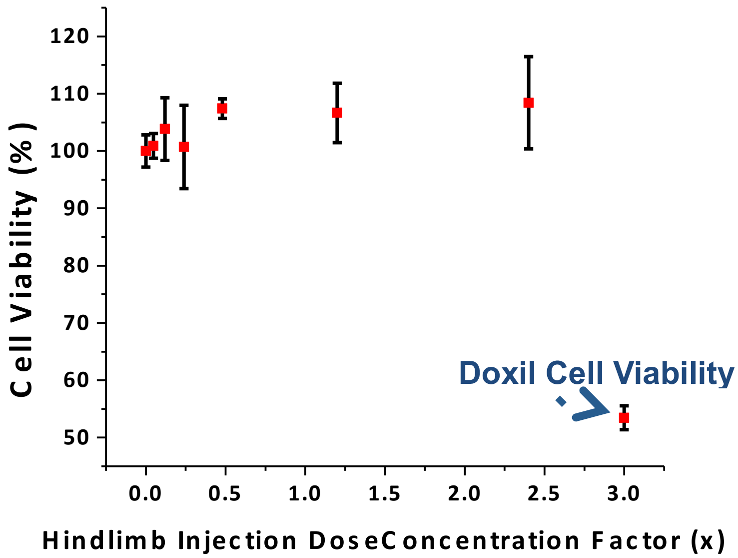

Figure S7: Preliminary cellular toxicity of CH1055-PEG. Cell toxicity was assayed utilizing the U87MG cell line. Cell viability was measured by quantifying the absorbance after the addition of Cell Titer 96. Viability was quantified by comparing the absorbance at each concentration to the absorbance of the positive control. Doxil was used as the negative control. The concentration was measured as a factor of the hindlimb injection concentration.

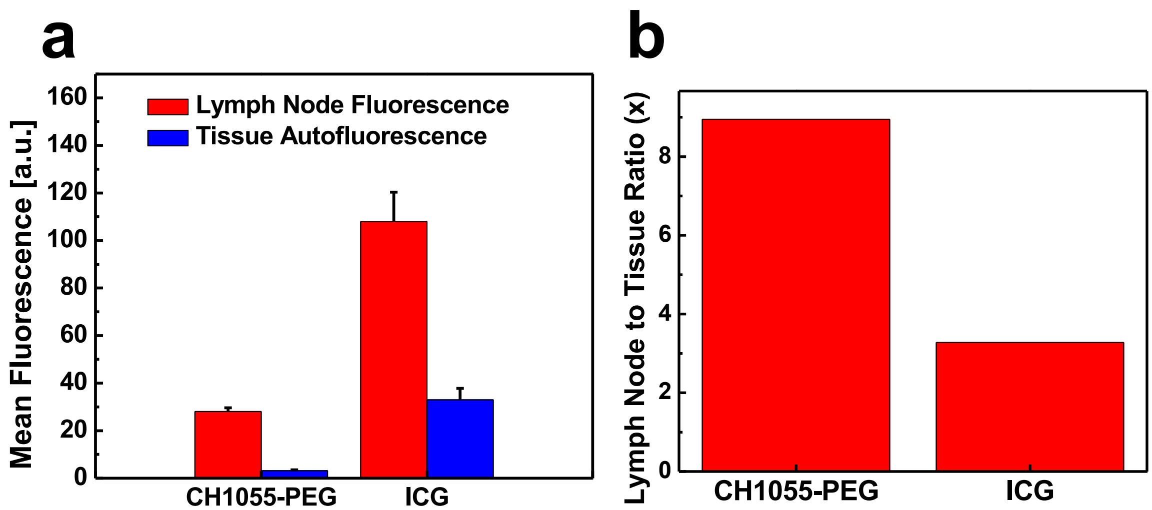

Supplemental Figure S8: Quantification of lymph node imaging in the NIR-I/II. (**a**) Inguinal lymph node fluorescence signal as well as background tissue autofluorescence levels ~1 hour post-injection of CH1055-PEG and ICG. (**b**) Lymph node-to-background tissue autofluorescence ratio (SBR) for CH1055-PEG and ICG. All values were normalized to compensate for differences in exposure time (CH1055-PEG: 300 ms; ICG: 50 ms).

As ICG has a higher quantum yield than CH1055-PEG, the ICG lymph node (LN) fluorescence intensity was markedly higher than that of CH1055-PEG yet the tissue background (TB) autofluorescence levels were >10x lower in the NIR-II. This resulted in a ~2x higher CH1055-PEG LN/TB ratio in comparison to ICG. While the clarity and image sharpness of imaging in the NIR-II with CH1055-PEG is drastically better than NIR-I imaging with ICG, these results indicate that CH1055-PEG can also improve surgeons abilities to differentiate lymph nodes from the surrounding tissue even though it has a lower quantum yield than ICG.

S9: ICG-PEG vs ICG for lymphatic vasculature imaging

To a solution of ICG-maleimide (0.5mg, 0.454 μmol, Dojindo Molecular Technologies) in 200 μL DMSO was added PEG-SH (9.08 mg, 4.54 μmol, M.W. 2000, Laysan Bio). The reaction mixture was stirred 12h at room temperature then purified by

Amicon Ultra-0.5mL 3k (washed 6 times). The purity of ICG-PEG was controlled by HPLC (Thermo Scientific Hypersil GOLD C4 column). The final product ICG-PEG was confirmed using MALDI-TOF-MS. Expected M.W. ~3000, Measured M.W. ~3000

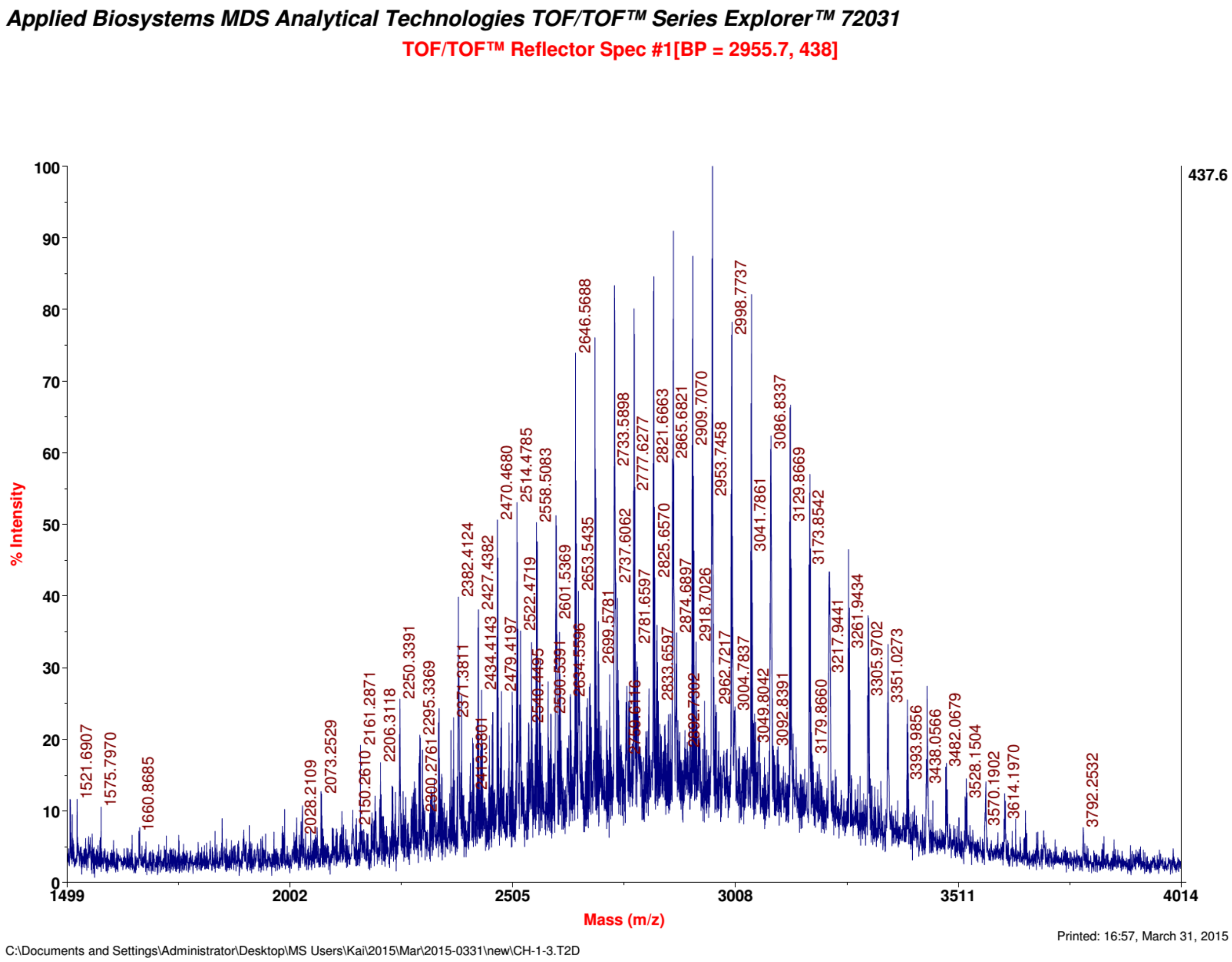

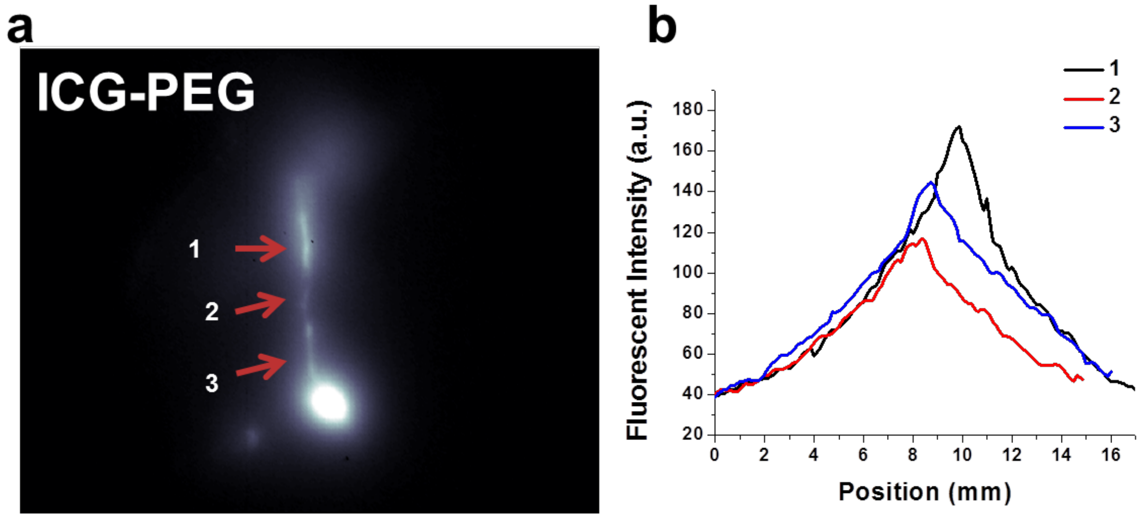

Supplemental Figure S9: Lymphatic vasculature imaging with ICG-PEG. (a) NIR-I fluorescence image (20 ms) after an ICG injection in a nude mouse (n=2) showing the popliteal lymph node and the internodal lymphatic vasculature. Numbered arrows correspond to the location and the direction of cross-sectional fluorescence intensity profiles in the (**b**) NIR-I region.

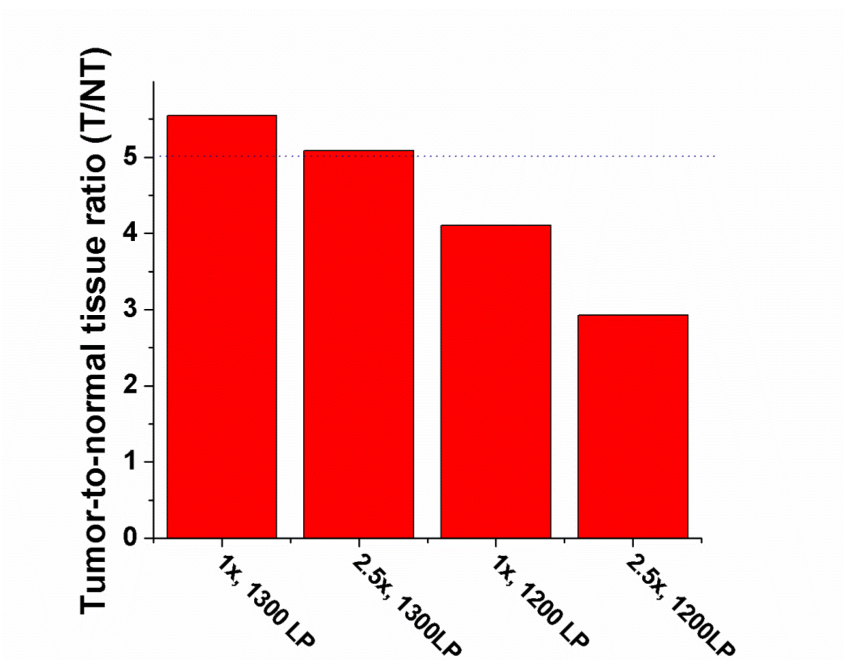

Figure S10: NIR-IIa fluorescence imaging of the U87MG brain tumor. The tumor-to-normal tissue ratio for brain tumor imaging with CH1055-PEG was quantified with a variety of magnifications and filters. While lower exposure times are needed when utilizing a 1200 nm long-pass filter, the use of a1300 nm long-pass filter provides a quantifiable improvement in imaging quality. Above, the 1x (magnification for the whole body set-up) shows a higher T/NT ratio than the 2.5x (magnification for the brain, hindlimb set-up) due to the lower magnification. Furthermore, it was not possible to achieve a signal-to-background ratio (SBR) above 5 (demarcated with a dotted blue line) which would meet the Rose criterion, when utilizing a 1200 LP filter. An SBR above 5 was only achievable with a 1300 nm long-pass filter.

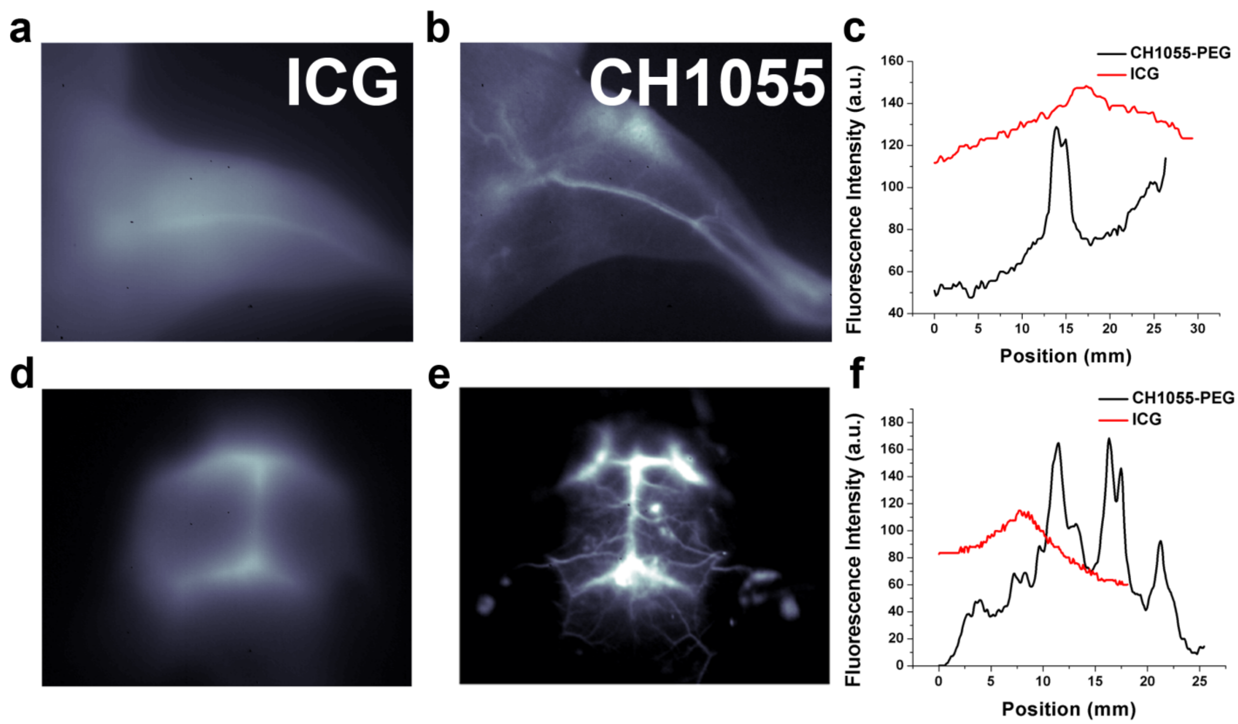

Figure S11: *In vivo* NIR-II vascular fluorescence imaging with CH1055-PEG and ICG in mice. Hindlimb vascular imaging with (**a**) ICG and (**b**) CH1055-PEG to compare imaging quality with NIR-I and NIR-II fluorescence imaging. (**c**) Representative fluorescent cross-sectional profiles for both ICG and CH1055-PEG taken perpendicular to the femoral artery. Brain vascular imaging with (**d**) ICG and (**e**) CH1055-PEG. (**f**) Representative fluorescent cross-sectional profiles for both ICG and CH1055-PEG taken perpendicular to the superior sagittal sinus. ICG was imaged between 850-900 nm with a 75 ms exposure time and CH1055-PEG was imaged with a 1200 LP filter and a 200 ms exposure time for the hindlimb and a 1300 LP filter and 1s exposure time for the brain to allow imaging in the NIR-IIa region (1300-1400 nm).

While the resolution of fine vascular features in the brain was also performed with a 1200 LP filter at an exposure time of 200 ms, a representative image of NIR-IIa imaging is shown yet a longer exposure time is required. Since CH1055's emission peak is at ~1055 nm, fluorescence imaging at exposure times of <100 ms is possible with a 1000 nm filter. While utilizing a 1000 LP filter is still within the NIR-II window, the imaging quality significantly increases at progressively longer wavelengths yet slightly, yet still reasonable, exposure times are required. Intensity cross-sectional profiles clearly demonstrate the advantages of NIR-II imaging as small vessels clearly appear when utilizing CH1055-PEG, yet no fine features can be resolved with ICG other than the main femoral vessels and the superior sagittal sinus. Interestingly, the cross-sectional profile for the hindlimb when utilizing CH1055-PEG displays two peaks corresponding to the artery and the vein, both of which can be clearly resolved in the image.

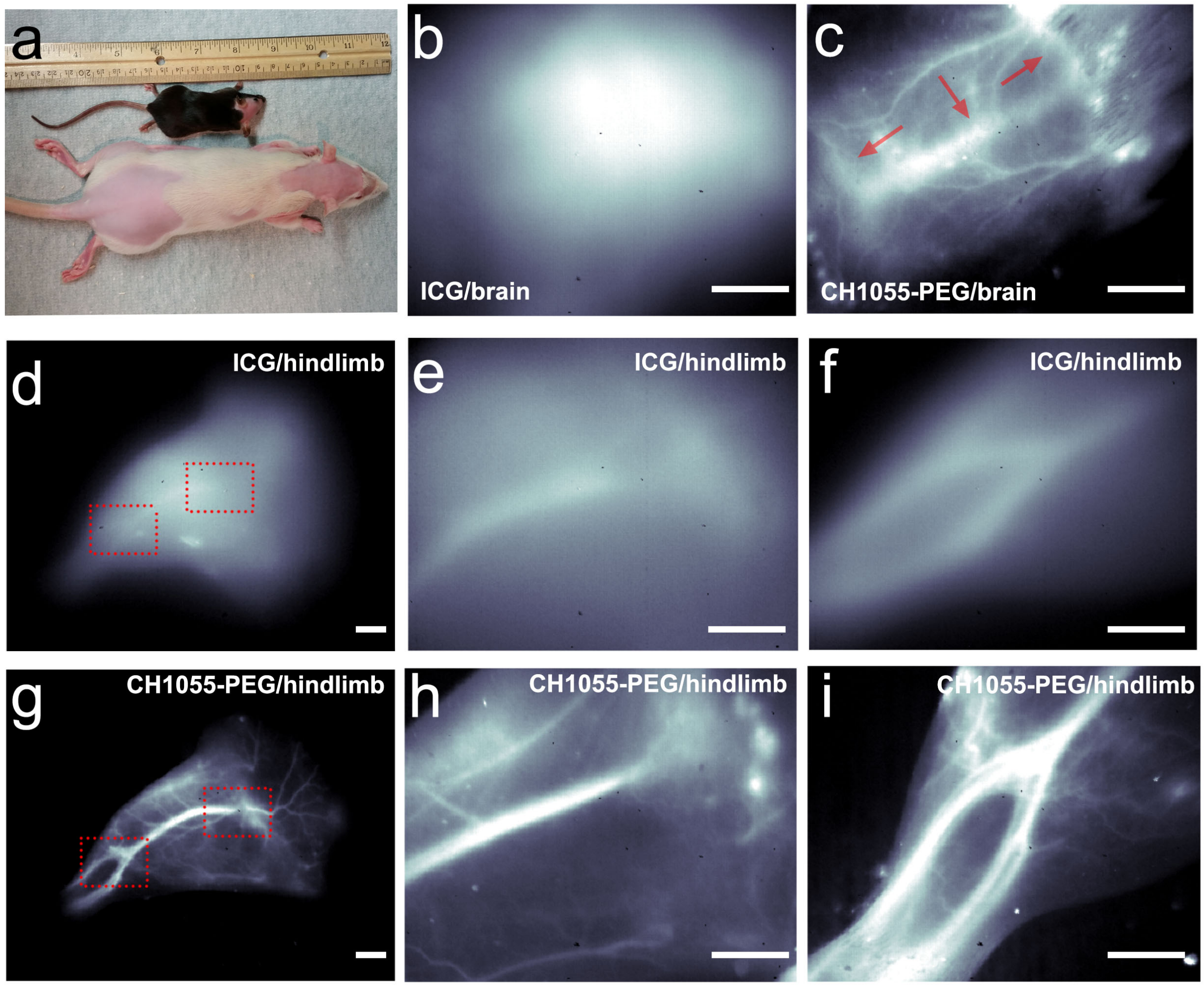

Figure S12: *In vivo* NIR-II vascular fluorescence imaging with CH1055-PEG and ICG in rats. (**a**) Photograph of a rat (250 g) side-by-side to a typical mouse for comparison. Both animals have been shaved for prior imaging. (**b**) ICG and (**c**) CH1055-PEG rat brain imaging under 2.5x magnification. Red arrows correspond to the inferior cerebral vein, the superior sagittal sinus, and the transverse sinus. NIR-I and NIR-II hindlimb imaging in rats under the (**d**),(**g**) 1x whole body setup and (**e-f**),(**h-i**) 2.5x setup, respectively. Zoomed-in locations with the 2.5x-magnified setup are denoted with the red dotted rectangles in the corresponding 1x whole body image. All imaging was performed ~1-10 minutes post-injection of 0.5 mg/kg ICG (40 ms exposure, 850-900 nm) and 4 mg/kg CH1055-PEG (400 ms exposure, 1200LP).

After an intravenous injection of ICG in the NIR-I in mice, the blurred femoral vessels can be hardly differentiated from the surrounding tissue for the length of the hindlimb yet in rats. Conversely, in the NIR-II, CH1055-PEG produced the clear, crisp images of the rat hindlimb vasculature as expected (see Supplemental Fig. S12g-i). Further, we performed imaging of the rat brain. In the NIR-I in rats, we observed not even blurred vessels in the rat brain (Supplemental Fig. S12b), which is a far departure from mice brain NIR-I imaging (Fig. 4g) where blurred inferior cerebral vein, the superior sagittal sinus, and the transverse sinus are visible. In contrast, imaging in the NIR-II with a 1200 nm long-pass filter, CH1055-PEG allowed visualization of all of these vessels with much higher clarity (Supplemental Fig. S12c).

Section S13: Characterization of CH1055-affibody conjugation.

Dissolve CH1055 (0.603 mg, 0.622 umol) and 10 ul DIPEA into 200 ul of anhydrous DMSO. Then add N-(2-Aminoethyl) maleimide hydrochloride (0.0111 mg, 0.622 umol), TSTU (0.0206 mg, 0.6842 umol) into the CH1055 solution. Keep reacting 6 h at room temperature. After the reaction is finished, dilute with water. Adjusting the pH to 7 with 0.1M HCl. Then add the affibody (4.354 mg, 0.622 umol) (TCEP pretreat) into the reaction solution and react over night under N_2 protection. Finally, use a HPLC column to purify to get the final product: CH1055-affibody 2mg. Yield 40%.

CH1055-$Z_{EGFR:1907}$

Expected M.W. 7780.8

Measured M.W. 7787.9

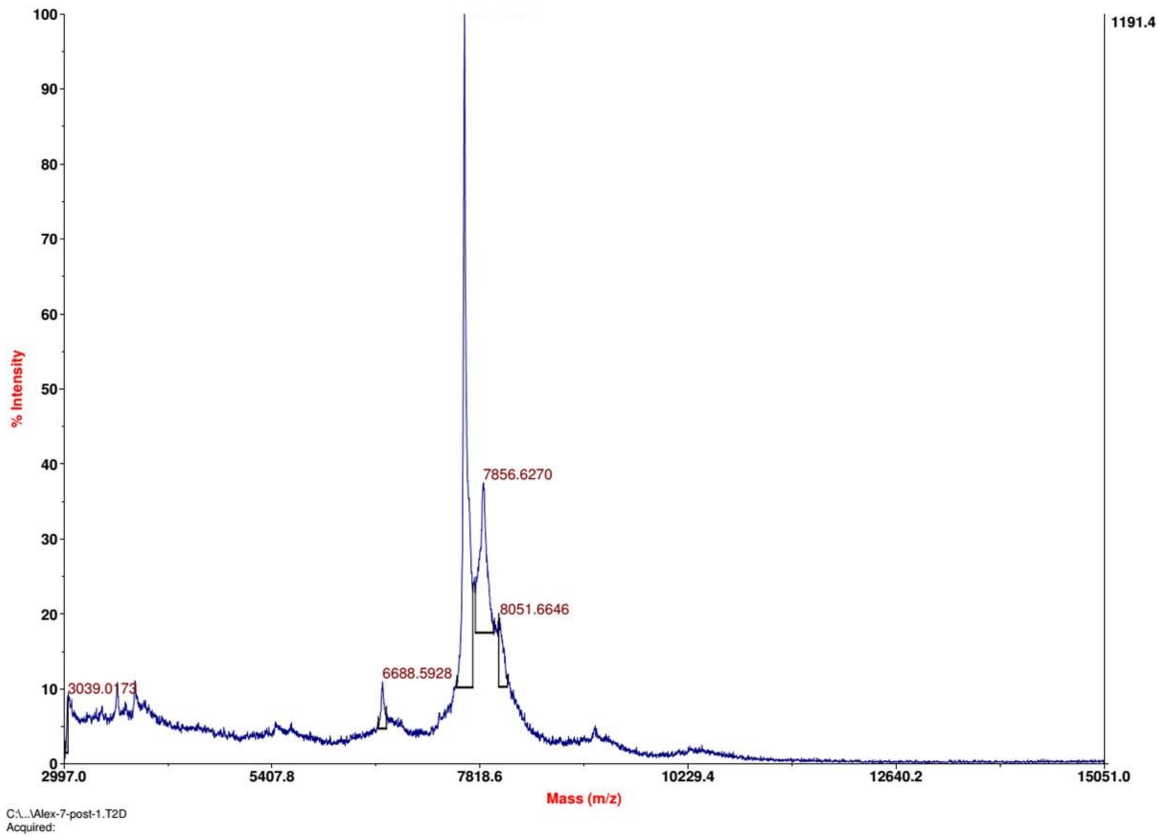

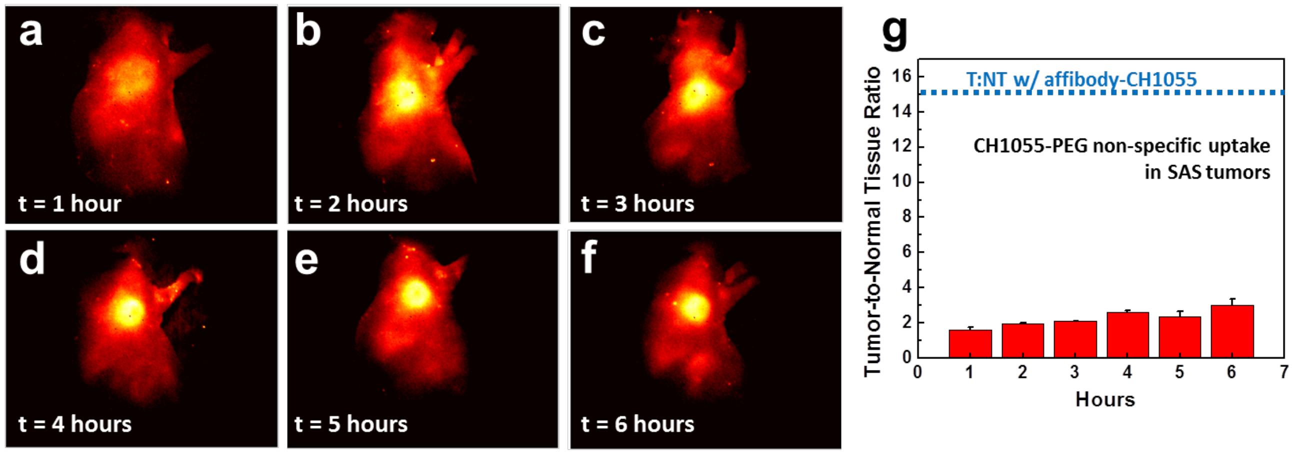

Supplemental Figure S14: Tumor imaging through non-specific uptake of CH1055-PEG. Imaging time-points at **(a)** 1 hour **(b)** 2 hours **(c)** 3 hours **(d)** 4 hours **(e)** 5 hours **(f)** and 6 hours post intravenous injection of CH1055-PEG in 3 nude mice expressing xenographt SAS tumors (1200 LP, 400 ms). **(g)** Tumor-to-normal tissue ratio of non-specific uptake of CH1055-PEG. The blue line indicates the approximate T/NT of the CH1055-affibody during the same time window.

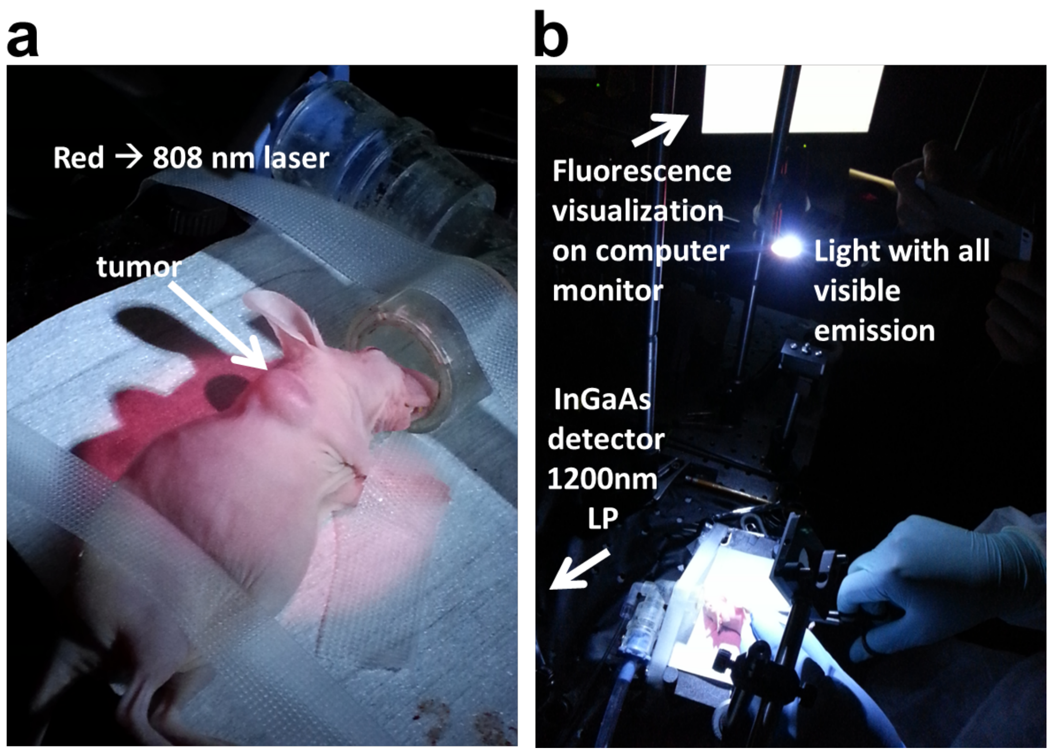

Supplemental Figure S15: CH1055-affibody guided-surgery NIR-II fluorescence imaging setup. (**a**) Photograph showing a nude mouse expressing a xenograft SAS tumor targeted with CH1055-affibody. Red light corresponds to the minimal visible red light emission of the 808 nm laser and penciled outline corresponds to the imaging field of view. (**b**) Photograph of the entire imaging setup showing a guided-surgery in progress where the mouse is illuminated with a white light that has no emission at longer wavelengths. The InGaAs imaging setup is immediately in front of the surgical surface with a right angle mirror reflecting fluorescence emission into the NIR-II detection optics. The computer monitor displaying the fluorescent images is immediately to the right of the surgical surface.

C. NMR Spectrum

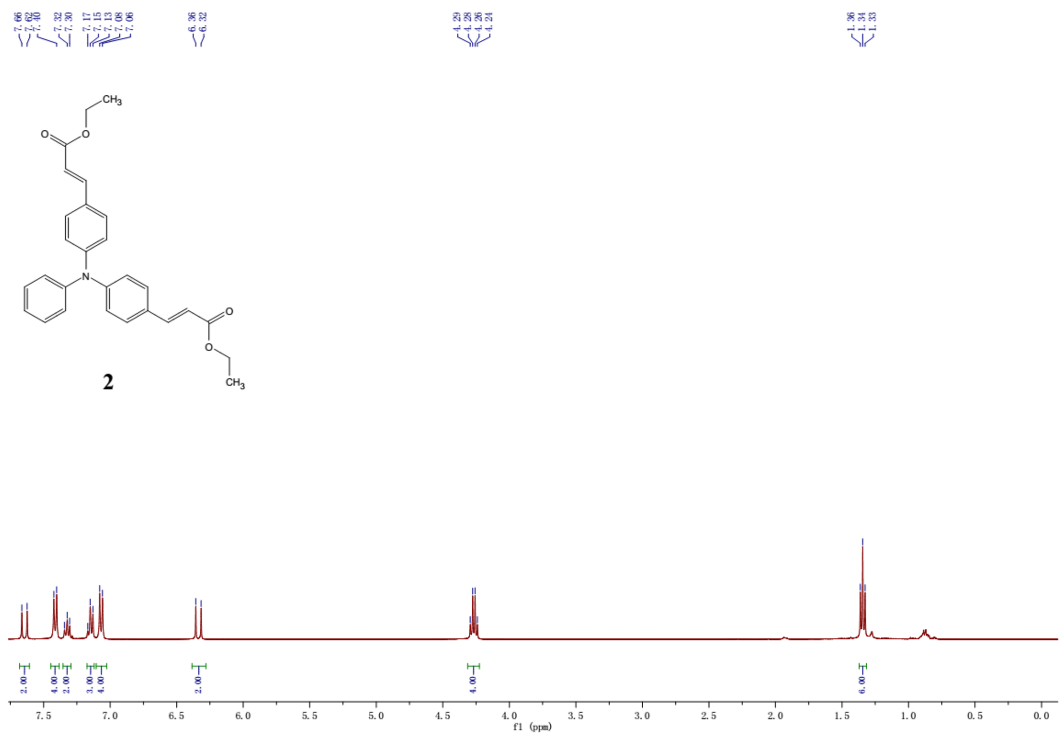

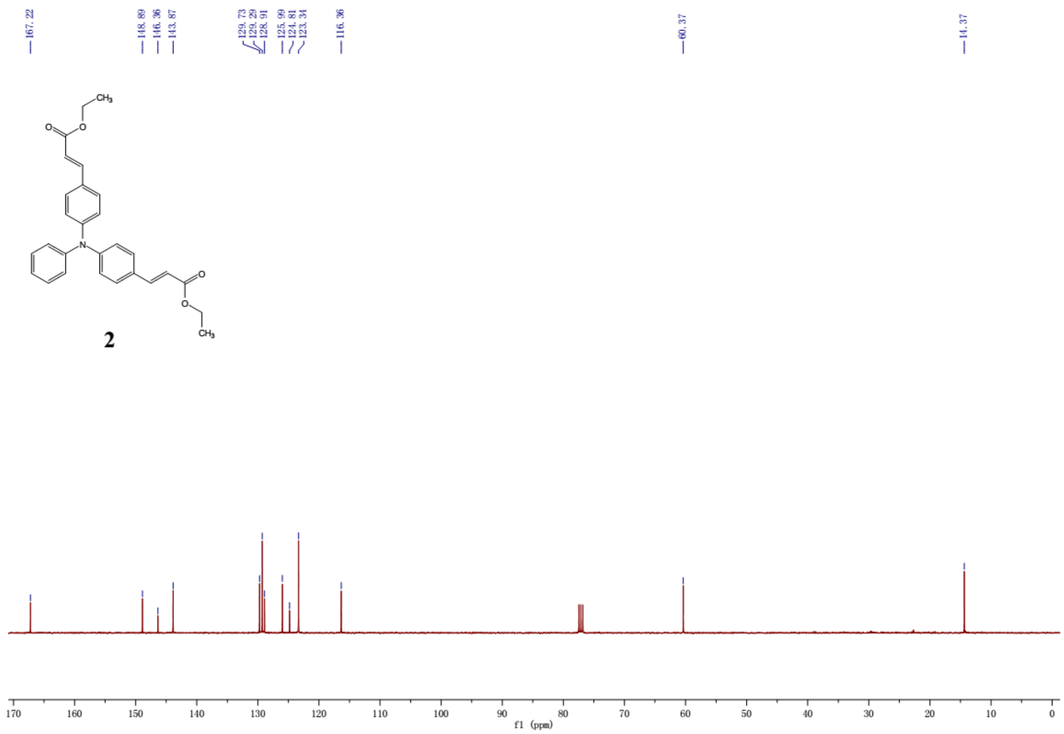
167.22
148.89
146.36
143.87
129.73
129.29
128.91
125.99
124.81
123.34
116.36
60.37
14.37
f1 (ppm)

2

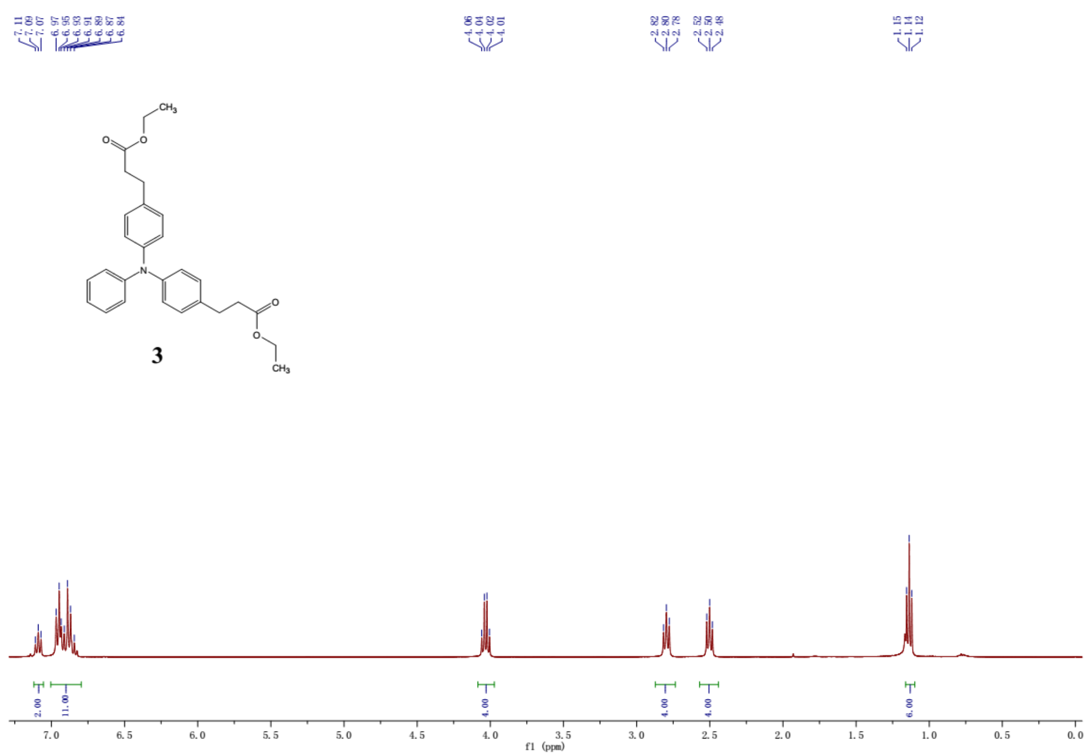
7.11
7.09
7.07
6.97
6.95
6.93
6.91
6.89
6.87
6.84
4.06
4.04
4.02
4.01
2.82
2.80
2.78
2.52
2.50
2.48
1.15
1.14
1.12
2.00
11.00
4.00
4.00
4.00
6.00
f1 (ppm)

3

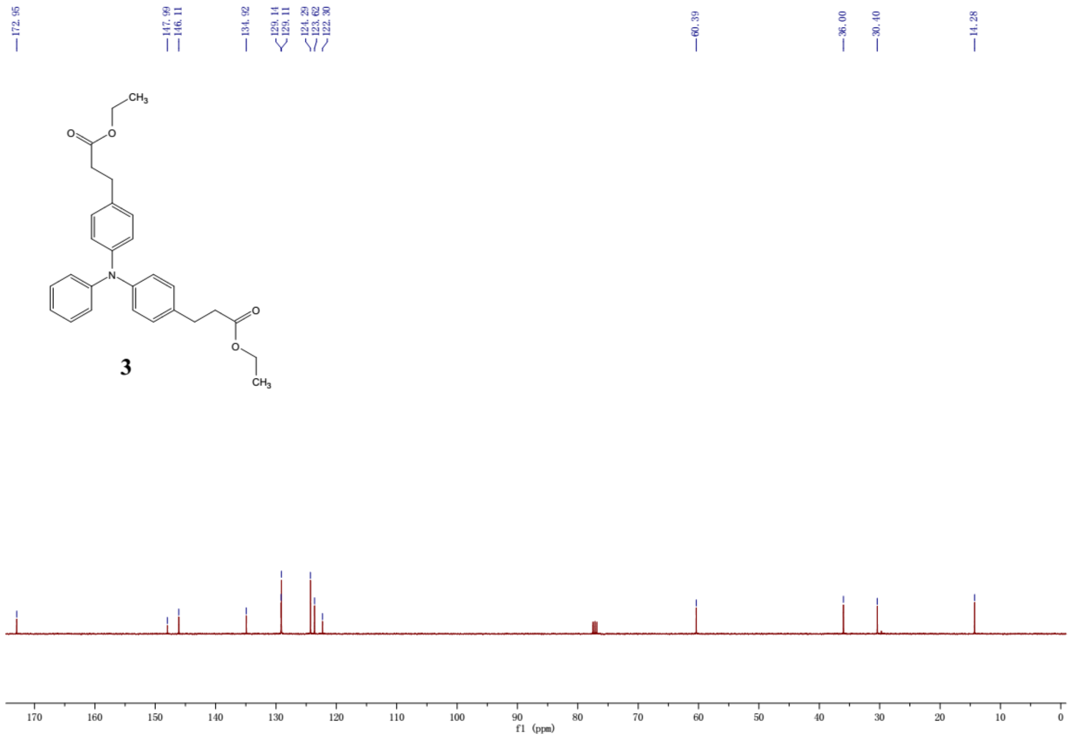
172.95
147.99
146.11
134.92
129.14
129.11
124.29
123.62
122.30
60.39
36.00
30.40
14.28
CH3
O
O
N
O
O
CH3
170 160 150 140 130 120 110 100 90 80 70 60 50 40 30 20 10 0
f1 (ppm)
3


7.27
7.24
7.07
7.05
6.98
6.97
6.95
6.88
6.86
4.15
4.14
4.12
4.10
2.91
2.89
2.87
2.62
2.60
2.58
1.25
1.23
1.21
H3C
O
O
N
Br
H3C
O
O
2.00
4.00
4.00
2.00
4.00
4.00
4.00
6.00
7.0 6.5 6.0 5.5 5.0 4.5 4.0 3.5 3.0 2.5 2.0 1.5 1.0 0.5 0.0
f1 (ppm)
4

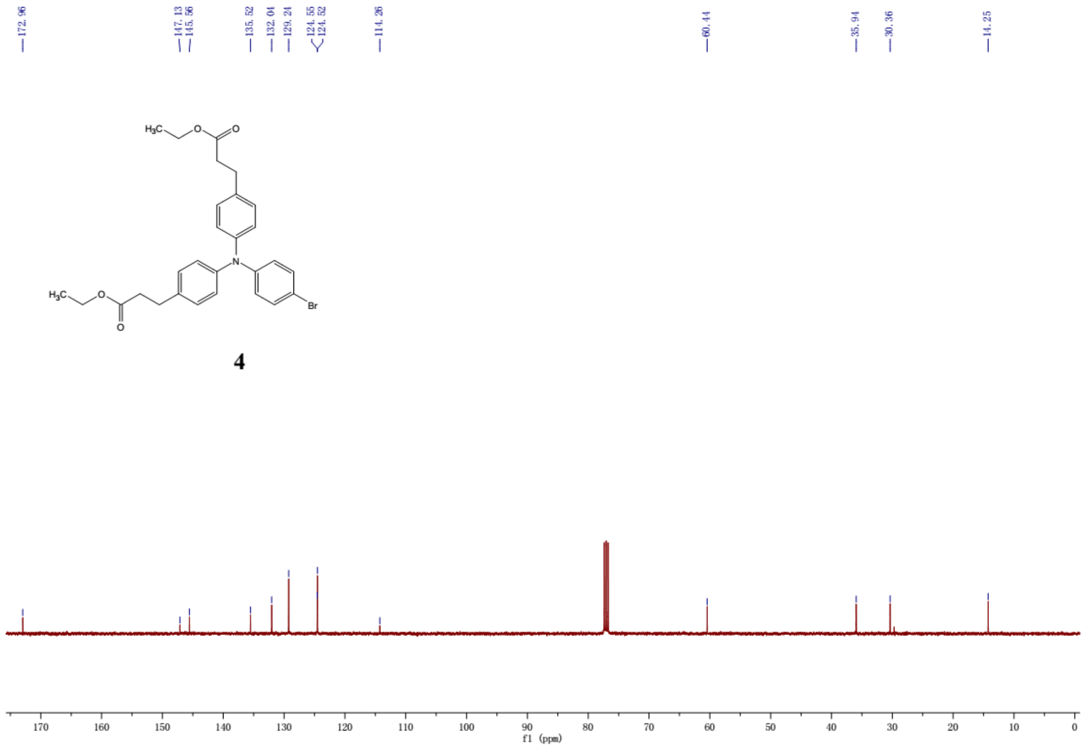

172.96
147.13
145.56
135.52
132.04
129.24
124.55
124.52
114.26
60.44
35.94
30.36
14.25
H_3C
O
O
N
Br
4
170 160 150 140 130 120 110 100 90 80 70 60 50 40 30 20 10 0
f1 (ppm)

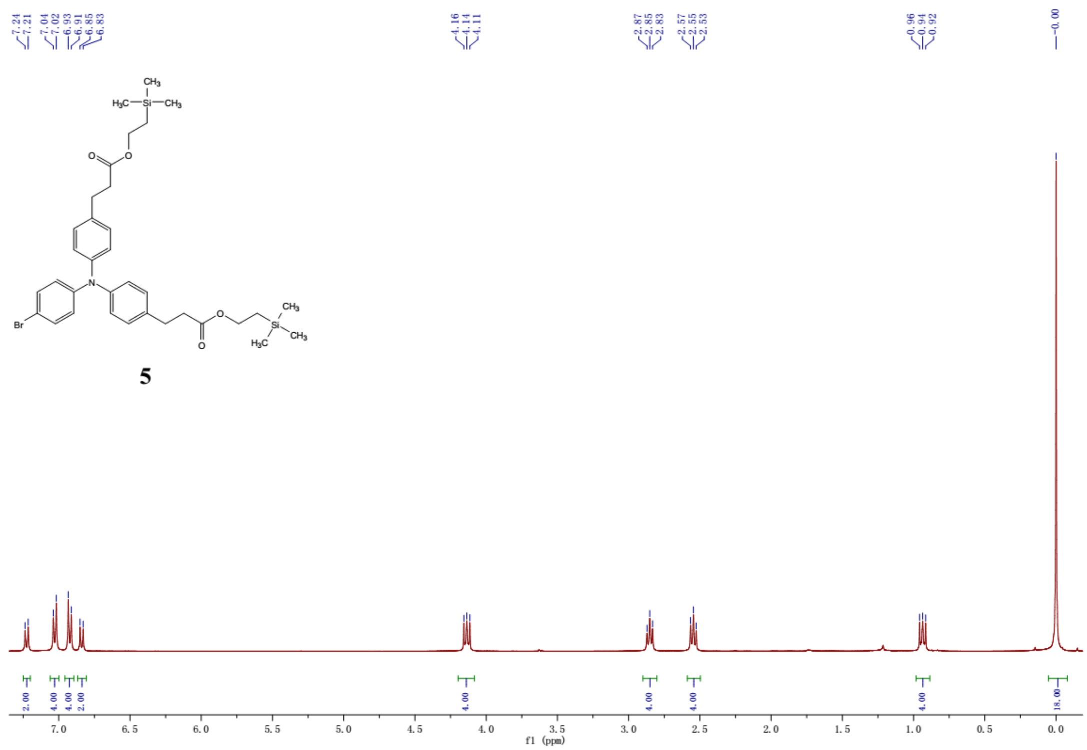

7.24
7.21
7.04
7.02
6.93
6.91
6.85
6.83
4.16
4.14
4.11
2.87
2.85
2.83
2.57
2.55
2.53
0.96
0.94
0.92
0.00
CH_3
H_3C
Si
CH_3
O
O
N
Br
5
2.00
4.00
4.00
2.00
4.00
4.00
4.00
4.00
18.00
7.0 6.5 6.0 5.5 5.0 4.5 4.0 3.5 3.0 2.5 2.0 1.5 1.0 0.5 0.0
f1 (ppm)

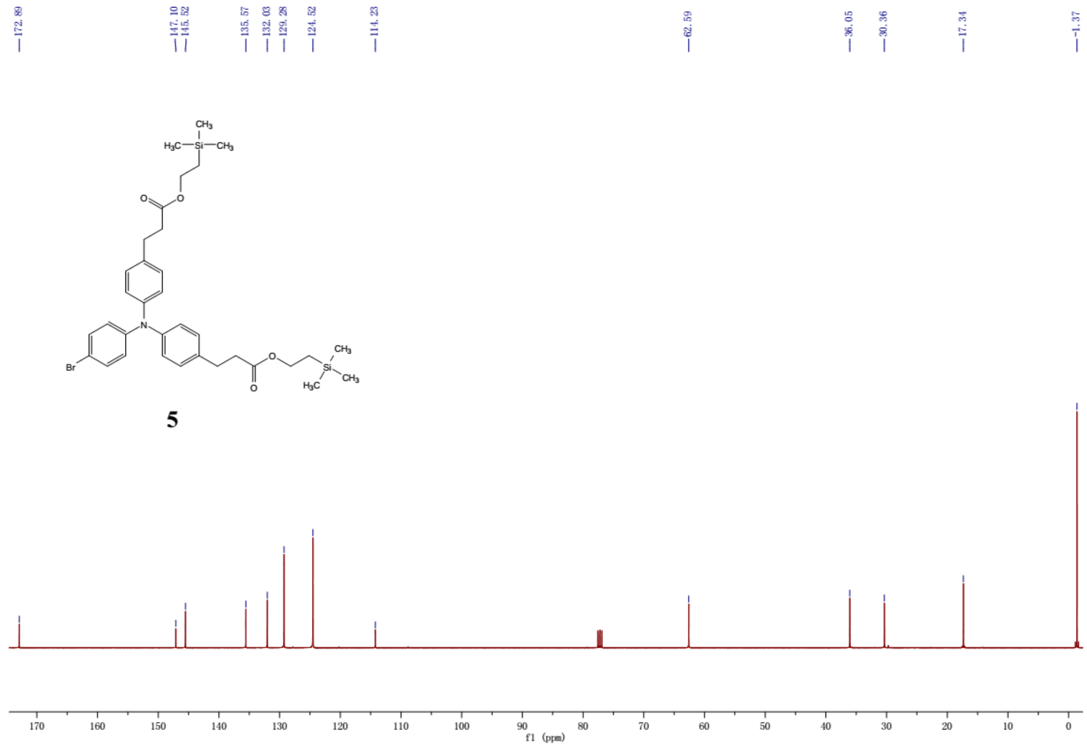
172.89
147.10
145.52
135.57
132.03
129.28
124.52
114.23
62.59
36.05
30.36
17.34
-1.37
f1 (ppm)

5

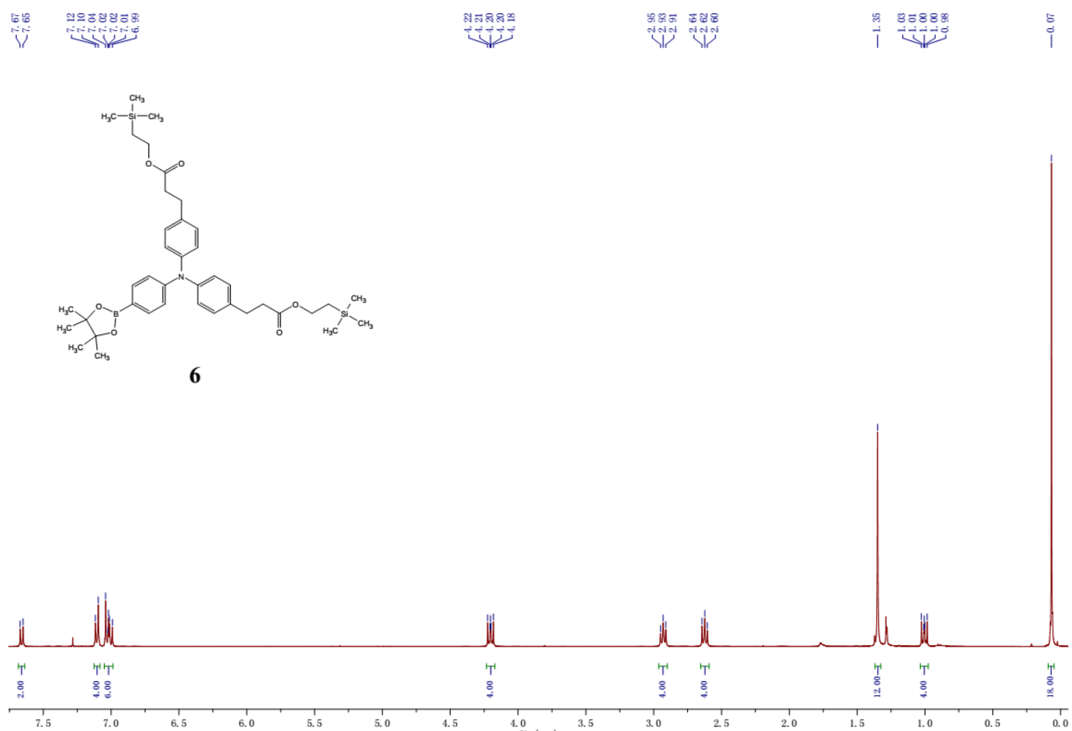
7.67
7.65
7.12
7.10
7.04
7.02
7.02
7.01
6.99
4.22
4.21
4.20
4.20
4.18
2.95
2.93
2.91
2.64
2.62
2.60
1.35
1.03
1.01
1.00
1.00
0.98
0.07
2.00
4.00
6.00
4.00
4.00
4.00
12.00
4.00
18.00
f1 (ppm)

6

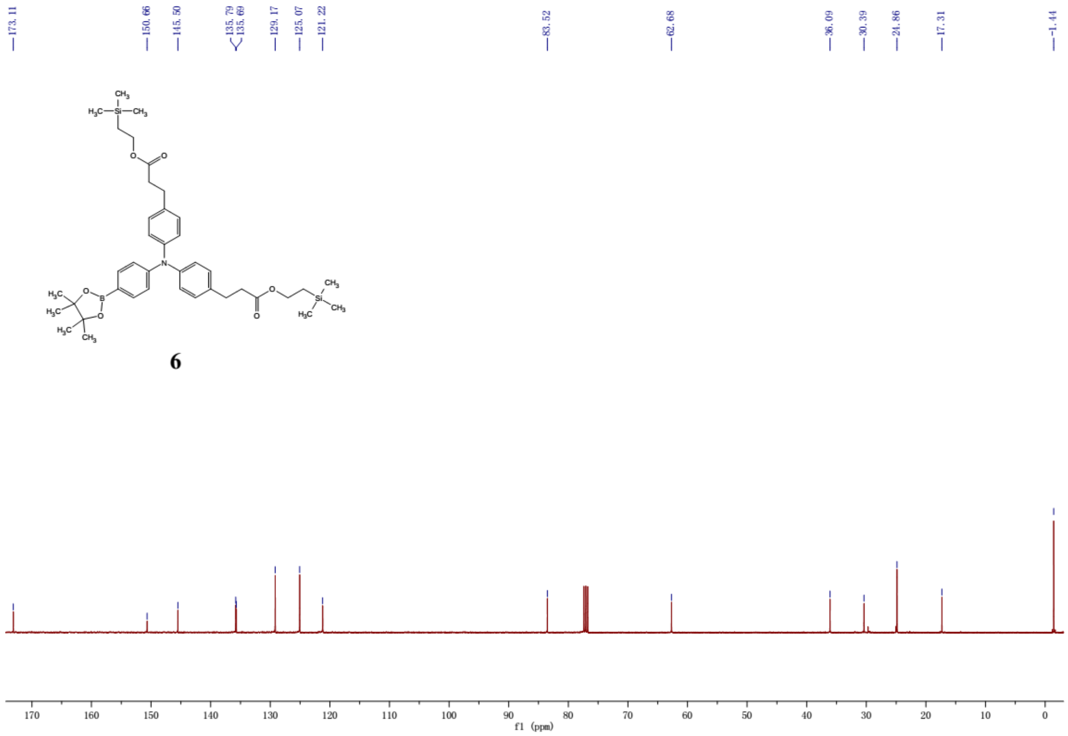
173.11
150.66
145.50
135.79
135.69
129.17
125.07
121.22
83.52
62.68
36.09
30.39
24.86
17.31
-1.44
6
f1 (ppm)

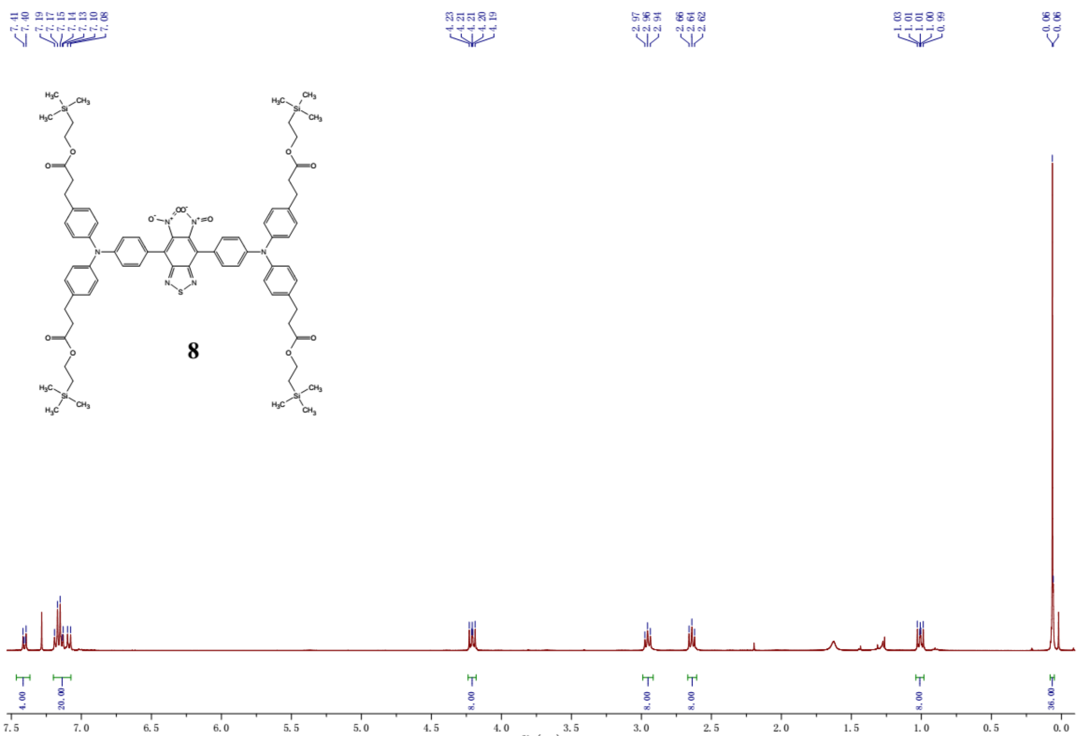
8
4.00
20.00
8.00
8.00
8.00
8.00
36.00
f1 (ppm)

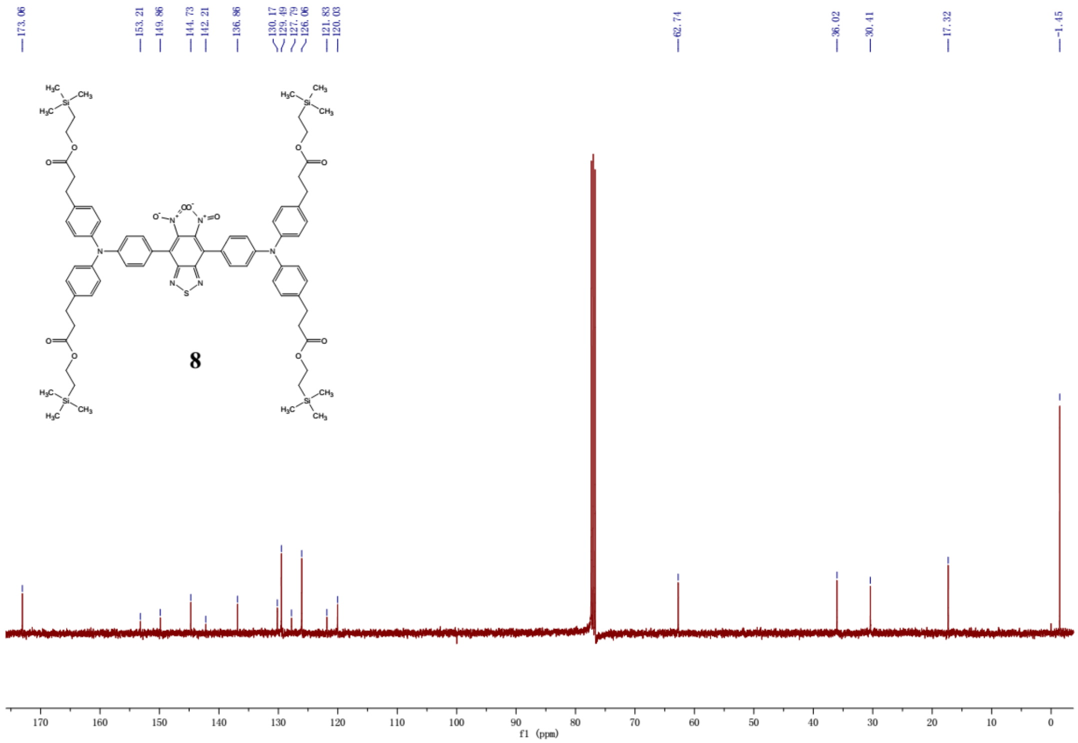
173.06
153.21
149.86
144.73
142.21
136.86
130.17
129.49
127.79
126.06
121.83
120.03
62.74
36.02
30.41
17.32
-1.45
8
f1 (ppm)

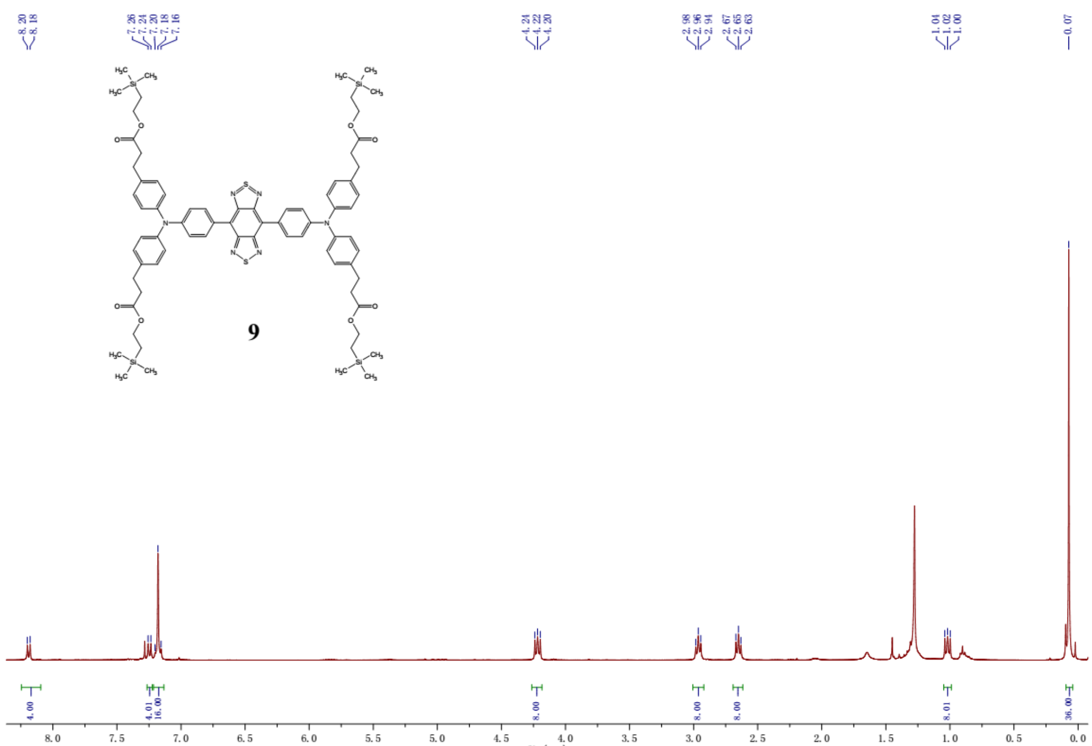
8.20
8.18
7.26
7.24
7.20
7.18
7.16
4.21
4.22
4.20
2.98
2.96
2.94
2.67
2.65
2.63
1.04
1.02
1.00
0.07
9
4.00
4.01
16.00
8.00
8.00
8.00
8.01
36.00
f1 (ppm)

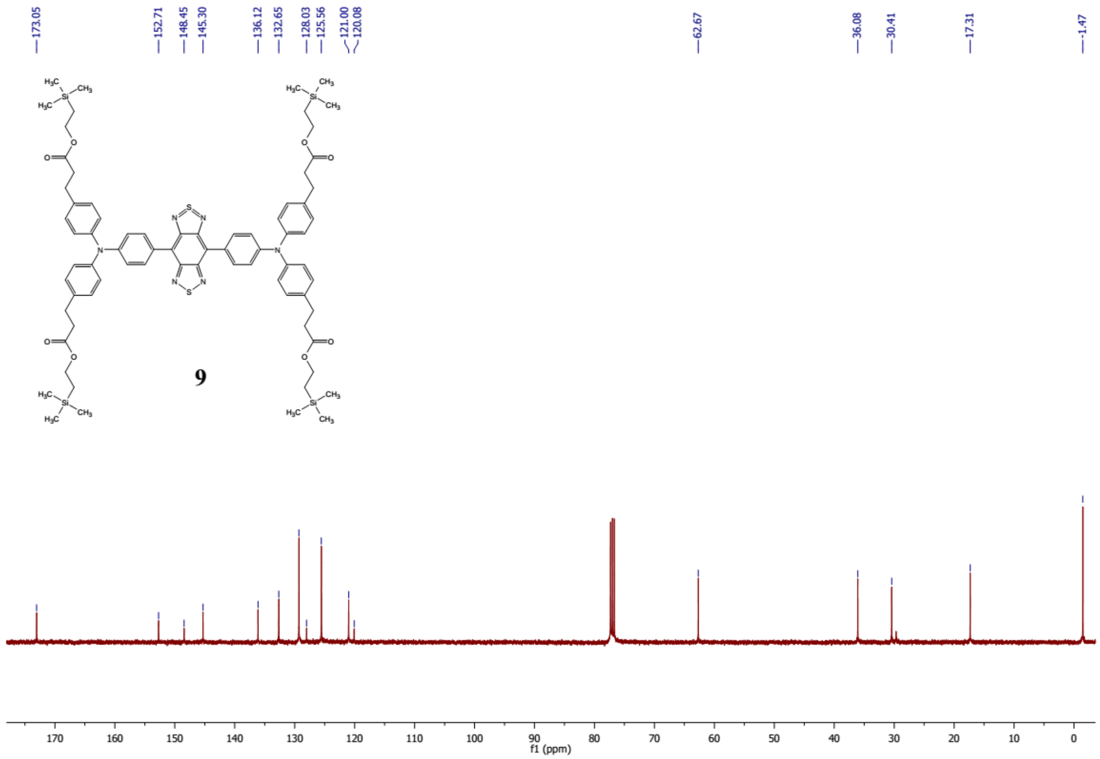
173.05
152.71
148.45
145.30
136.12
132.65
128.03
125.56
121.00
120.08
62.67
36.08
30.41
17.31
-1.47
9
f1 (ppm)

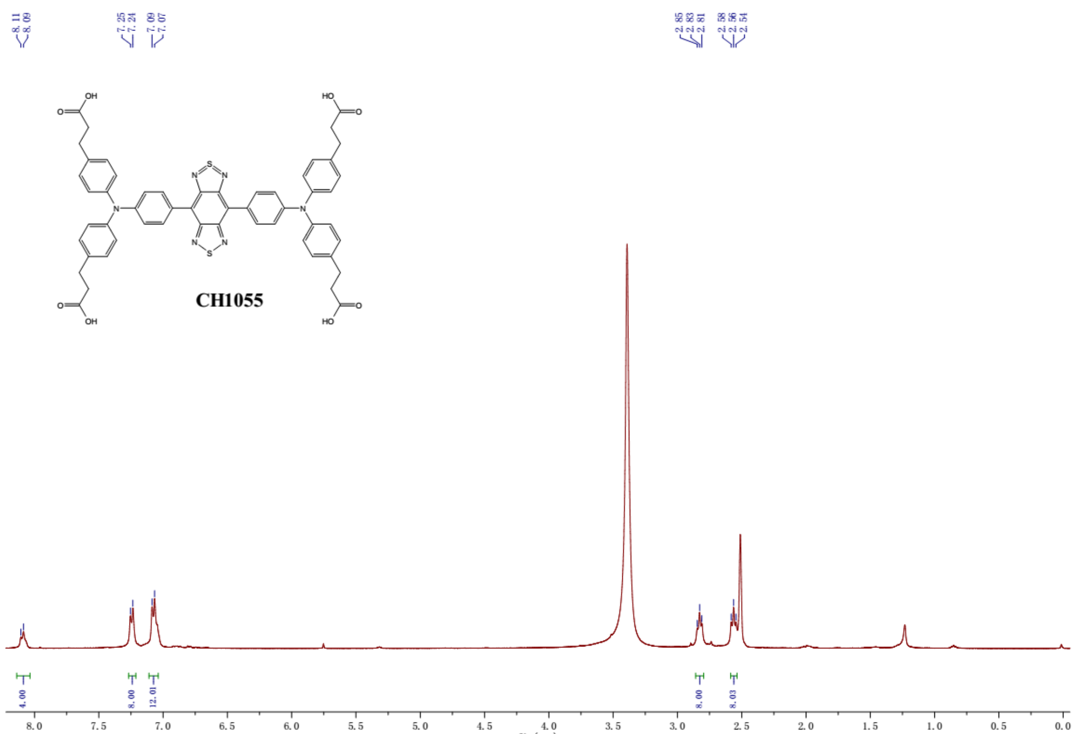
8.11
8.09
7.25
7.24
7.09
7.07
2.85
2.83
2.81
2.58
2.56
2.54
CH1055
4.00
8.00
12.01
8.00
8.03
f1 (ppm)

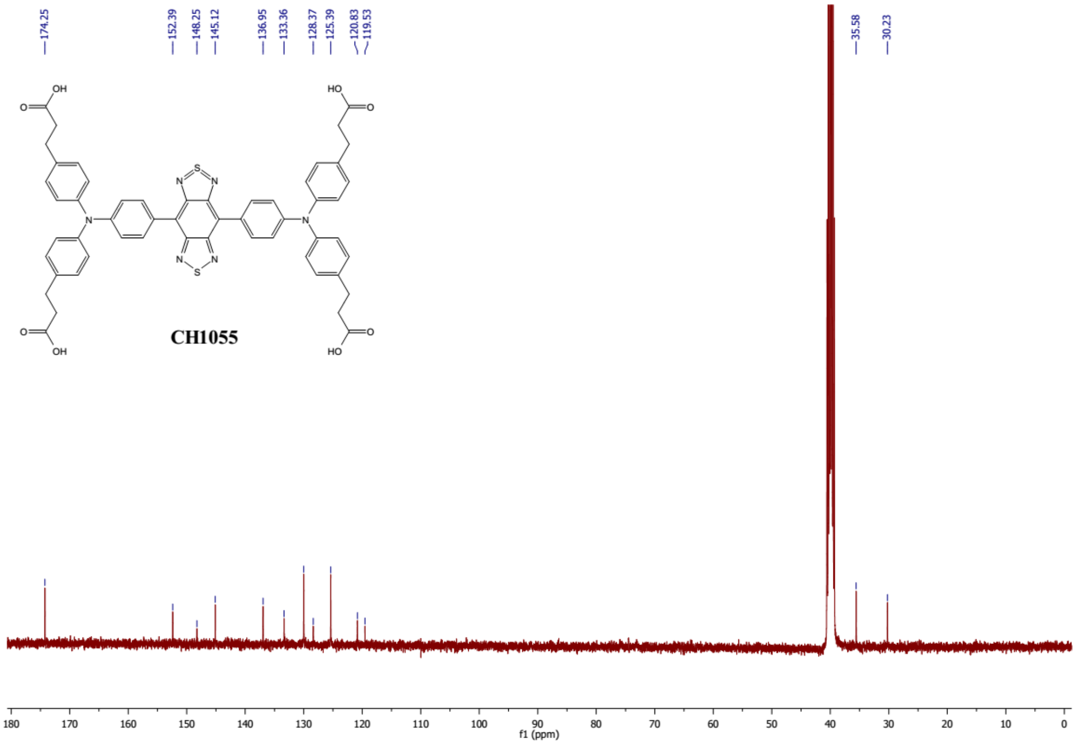

References:

1. Y. X. Wang, M. Leung, 4, 4′, 4′′-Tris(acetoxymethylene)triphenylamine: An Efficient Photoacid Promoted Chemical Cross-Linker for Polyvinylcarbozole and Its Applications for Photolithographic Hole-Transport Materials. *Macromolecules* **44**, 8771–8779 (2011).
2. T. Uno, K. Takagi, M. Tomoeda, Synthesis of bisfurazanobenzo-2,1,3-thiadiazole and related compounds. *Chem. Pharm. Bull.* **28**, 1909-1912 (1980).
3. Z. Cheng et al., ^{64}Cu-Labeled Affibody Molecules for Imaging of HER2 Expressing Tumors. *Mol. Imaging Biol.* **12**, 316-324 (2010).